Optimal fermion-qubit mappings

Mitchell Chiew¹ and Sergii Strelchuk¹

¹DAMTP, Centre for Mathematical Sciences, University of Cambridge, Cambridge CB30WA, UK (Dated: February 3, 2022)

Simulating fermionic systems on a quantum computer requires a high-performing mapping of fermionic states to qubits. The key characteristic of an efficient mapping is its ability to translate local fermionic interactions into qubit interactions. This has strong implications both on the number of qubits as well as the gate cost of simulations. We introduce a novel way to optimise fermion-qubit mappings by studying fermionic enumeration schemes. Finding an efficient enumeration scheme allows one to increase the locality of the target qubit Hamiltonian without expending any additional resources. The problem of finding optimal arrangements for a general fermionic connectivity graph is NP-complete. We find optimal enumeration schemes for fermionic lattices, which leads to qubit Hamiltonians with terms using 13.9% less gates than in previous methods. We also find efficient enumeration designs for a range of other practical connectivities where for n fermions we achieve $n^{\frac{1}{4}}$ improvement. A further advantage of our scheme for fermionic lattices is that by adding only two ancilla qubits we can reduce the average gate count of Hamiltonian terms by a full 40% compared to previous methods.

I. INTRODUCTION

Simulating physical systems is one of the most promising applications of quantum computers. Fermionic systems, encountered in many fields of theoretical and experimental physics, ranging from quantum physics to condensed matter to quantum field theories, pose a complex, often intractable computational challenge when studied with the aid of classical computers. These include, for example, the electronic structure problem, studying properties of gauge theories that govern strong interactions between quarks and gluons, determining ground state properties of fermionic Hamiltonians and many others.

There have been a number of recent developments in quantum computing that could make solutions to the above questions feasible [1–7]. However, many of these approaches [1, 7] rely on phase estimation [8, 9] and in turn require an impractically large number of qubits and quantum gates in order to keep the register of the quantum computer coherent [10]. Even those algorithms designed for near-term quantum computers, such as variational quantum eigensolvers [2, 10, 11], are beyond the reach of current technology. Furthermore, studying fermionic systems in 2D or 3D greatly amplifies these difficulties because of the overwhelming number of local fermionic interactions which become non-local once mapped in the qubit picture. The first mapping in 2D was introduced by Verstraete and Cirac [12], which is still widely used despite giving rise to highly non-local terms in the absence of ancilla qubits.

To bring the problem of fermionic simulation closer to meeting constraints of near-term quantum technology, it is crucially important to establish protocols that find optimal (in a certain well-defined sense) tradeoffs between the locality of the fermionic interactions and the locality of the corresponding interactions once mapped onto qubits. This is a complex challenge that largely has not been met with much progress because the formalisa-

tion of simulating fermionic interactions in a complexitytheoretic sense has has been extraordinarily difficult.

One can break down all quantum algorithms for fermionic simulation into three sequential steps: initialising the quantum register, applying unitary gates to the qubits, and measuring the result to obtain an estimate for the desired molecular property or other quantity of interest. Within this framework, algorithms may encode the fermionic Hamiltonian via first or second quantisation. Fermi-Dirac statistics impose asymmetry on fermionic systems' wavefunctions, and using first quantisation of the system's Hamiltonian, one can incorporate this asymmetry into the qubit basis itself or use the qubits to directly encode the wavefunction into real-time and realspace [1, 3, 4, 7]. Second quantisation encodes the asymmetry into the qubit operators rather than the quantum states [2]. This method necessitates a fermion-qubit mapping, to preserve the properties of fermionic creation and annihilation operators.

In our work, we focus on second quantisation because it provides a number of advantages over representations in the first quantisation [12, 13]. In the second quantisation picture Hamiltonians comprise products of fermionic creation and annihilation operators; a quantum algorithm must map each term of the Hamiltonian into a sequence of unitary gates acting on qubits. This transforms the original problem into a k-local Hamiltonian problem, where the size of k depends on the choice of fermion-qubit mapping. While in general, the local Hamiltonian problem is QMA complete [14], numerous attempts to reduce the complexity of this problem include using additional auxiliary qubits [12, 15, 16] in improved fermion-qubit mappings. Auxiliary qubits decrease non-locality of the qubit Hamiltonian, substantially reducing the complexity, and making small instances of a problem within reach of fairly modest quantum computers.

The idea of fermion-qubit mappings originates in the work of Jordan and Wigner almost a century ago [17]. In recent years, there have been a flurry of results intro-

ducing new fermion-qubit mappings as well as generalising the existing ones to higher dimensions [15, 16, 18–20]. Nearly all of them work well in 1D, but experience impracticably large overheads in higher dimensions. To address this, one may consider adding auxiliary qubits [12, 16].

One entirely overlooked aspect of fermion-qubit mappings in higher dimensions is the use of the underlying fermion enumeration scheme. While trivial in 1D, it has the potential to dramatically improve the locality of the mapping in 2D and above. The type of lattice and the method of numbering fermions open up new avenues for optimising fermion-qubit mappings. Examining enumeration schemes, and finding the most efficient ones, we show how to increase the locality of the target qubit Hamiltonian without expending any additional resources. This directly translates into reductions for quantum gate count for Hamiltonian hopping terms. In our work, we will consider several figures of merit. One such central quantity, the *Pauli weight*, is the number of qubits involved in a string of Pauli operations.

We relate the problem of optimising the simulation of hopping terms of fermionic Hamiltonians to the task of minimising the average Pauli weight of the corresponding qubit Hamiltonians. In 2D, this relates to the edgesum problem from graph theory [21–24]. Through our analysis, the optimal solution of the edgesum problem emerges as a clear definition for the optimal ancilla-free fermion enumeration scheme. For the regular fermionic lattice using a Jordan-Wigner transformation, and when compared to the S-pattern introduced by Verstraete and Cirac [12], our method directly improves the locality of the gubit Hamiltonian and thus reduces the resources used by a quantum algorithm by a constant factor (\approx 13.9%). Our optimal fermion-qubit mapping uses a carefully selected enumeration scheme based on a special pattern recognised by Mitchison and Durbin in their seminal work [21]. The results of our work culminate in:

Theorem 1 [Informal]

Given a system of $n = N^2$ fermions interacting in a square $N \times N$ lattice, a fermion enumeration scheme which follows the Mitchison-Durbin pattern minimises the average Pauli weight of the hopping terms.

Our approach of choosing edge sum-minimising fermion enumeration schemes gives practical results beyond the case of the 2D lattice. For graphs of cellular arrangements of n fermions, our 'bespoke' enumeration schemes perform better than naïve alternatives by a factor of $\mathcal{O}(n^{1/4}),$ as Section IIID demonstrates. This implies that for particular families of graphs, it is highly likely that tailored enumeration schemes produce quantum circuits orders of magnitude shallower than one-size-fits all enumeration schemes, even without necessarily being the optimal solution to the edge sum problem.

The structure of the paper is as follows: in Section II we provide a self-contained introduction to fermion-qubit mappings and their implications on the gate count further specialised to Jordan-Wigner mapping. It is then

followed by results from complexity theory that will be used to prove our main result. In Section III we introduce fermion enumeration schemes, rigorous cost functions and show how to construct an optimal enumeration scheme in 2D. In Section IV, we explain the auxiliary qubit mapping technique and modify our fermion-qubit mapping to improve Theorem 1's 13.9% advantage over the S–pattern to nearly 40% using just two ancilla qubits. Finally, in Section V we place our self-contained result within the literature, and argue that our techniques suggest further opportunities to improve fermion-qubit mappings.

II. BACKGROUND

This section provides the necessary background for the Jordan-Wigner transformation on fermionic systems (Sections II A–II D), and details relevant graph problems and complexity theory (Section II E).

A. Canonical commutation relations

In order to describe a system of n fermions, it is necessary to label each fermion with an integer from 1 to n. This is the first step of any fermion-qubit mapping, and here we call it the process of choosing a fermion enumeration scheme. The fermionic system has a state space, known as $Fock\ space$, with the occupancy number basis $\{|j_1, j_2, \ldots, j_n\rangle\ |\ j_i \in \{0, 1\}\}$ where j_i denotes the occupancy of the ith fermion. The annihilation operators a_i act on the fermionic vector space as

$$a_i|j_1...\underbrace{0}_{i\text{th place}}...j_n\rangle = 0$$
 (1)

$$a_i|j_1...\underbrace{1}_{i\text{th place}}...j_n\rangle = (-1)^{\sum_{k=1}^{i-1}j_k}|j_1...\underbrace{0}_{i\text{th place}}...j_n\rangle,$$
 (2)

while their Hermitian conjugates a_i^{\dagger} are the creation operators, and act on the system accordingly. Equations 1 and 2 are equivalent to Equations 3, 4 and 5 [25], which are the fermionic anticommutation relations:

$$\{a_i, a_k\} = 0 \tag{3}$$

$$\{a_i^{\dagger}, a_k^{\dagger}\} = 0 \tag{4}$$

$$\{a_j, a_k^{\dagger}\} = \delta_{jk} \mathbb{1} . \tag{5}$$

B. Fermion-qubit mappings

Consider a general Hamiltonian H which encodes the dynamics of a fermionic system,

$$H = \sum_{\alpha} h_{\alpha} O_{\alpha} \,, \tag{6}$$

Property	Basis states	Fundamental operators
n fermions	$ j_1, j_2, \dots, j_n\rangle$ $j_i = \text{occupancy}$	Ladder operators a_i , a_j^{\dagger} with $\{a_i, a_j^{\dagger}\} = \delta_{ij} \mathbb{1}$, $\{a_i^{(\dagger)}, a_j^{(\dagger)}\} = 0$; Physical $\propto a_i^{\dagger} a_j + a_j^{\dagger} a_i$
$m \ge n$ qubits	$ l_1, l_2, \dots, l_m\rangle$ $l_i = \mathrm{spin}$	Unitaries A_i, A_j^{\dagger} , $1 \leq i \leq n$, with $\{A_i, A_j^{\dagger}\} = \delta_{ij} \mathbb{1}$, $\{A_i^{(\dagger)}, A_j^{(\dagger)}\} = 0$

Table I: Basic building blocks of fermionic systems, and the equivalent properties that must apply to a system of qubits in order for it to simulate the fermions.

where each O_{α} is the product of an equal number of creation and annihilation operators, and the complex coefficients h_{α} ensure that H is Hermitian. To simulate the n fermions, we suppose that we have $m \geq n$ qubits at our disposal. The state of the qubit system can be written in terms of the basis $\{|l_1, l_2, \ldots, l_m\rangle \mid l_i \in \{0, 1\}\}$, where l_i denotes the value of the binary observable (say, z-component of spin) of the ith qubit. Developing a fermion-qubit mapping is tantamount to finding unitary operators $\mathbb{A}_i \in U(m)$ such that $\{\mathbb{A}_i^{\dagger}, \mathbb{A}_j\} = \delta_{ij}\mathbb{1}$ and $\{\mathbb{A}_i^{(\dagger)}, \mathbb{A}_i^{(\dagger)}\} = 0$, for $i, j \in \{1, 2, \ldots, n\}$.

Table I summarises the defining properties of fermionic systems and their analogues in qubit systems and Figure 1 illustrates a very general picture of an arbitrary fermion-qubit mapping. All known fermion-qubit mappings in the literature are a subset of the template described in these two figures.

The most widely-used fermion-qubit mappings, such as the Jordan-Wigner [17] and Bravyi-Kitaev [26] transformations, simulate n fermions with n qubits. A considerable repertoire of fermion-qubit mappings has developed in recent years, each with its own strengths and weaknesses. Mappings that use m>n qubits, e.g. [15, 16] transform Hamiltonian terms into chains of Pauli spin operators $(\sigma^x, \sigma^y, \sigma^z)$ and reduce the lengths of these chains with stabilisers involving auxiliary qubits. We discuss this process in Section IV, and give a novel example for simulating the fermionic lattice using m=n+2 qubits.

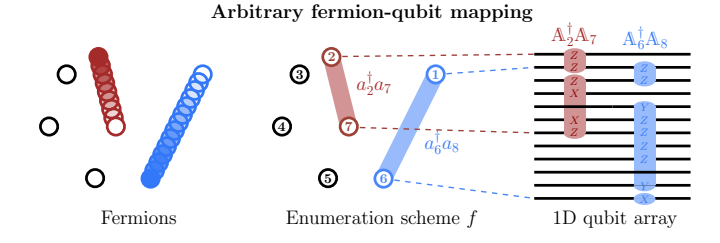


Figure 1: A fermion-qubit mapping uses a fermion enumeration scheme to describe interactions, such as $a_i^{\dagger}a_j$. Via the transformations $a_i \mapsto \mathbb{A}_i$, the fermion-qubit mapping replicates the algebra of the fermionic anticommutation relations on a system of $m \geq n$ qubits.

C. The Jordan-Wigner transformation

The Jordan-Wigner transformation uses m = n qubits and arises naturally by constructing

$$\sigma^{+} := \frac{1}{2}(\sigma^{x} - i\sigma^{y}) = \frac{1}{2}(X - Y) = |1\rangle\langle 0| \tag{7}$$

$$\sigma^{-} := \frac{1}{2}(\sigma^{x} + i\sigma^{y}) = \frac{1}{2}(X + Y) = |0\rangle\langle 1| , \qquad (8)$$

which behave somewhat like creation-annihilation operators in ket-bra form. Here, we use the convention $X = \sigma^x$ and $Y = i\sigma^y$. While $\{\sigma^+, \sigma^-\} = 1$, across multiple qubits when $i \neq j$ we have $\{\sigma_i^+, \sigma_j^-\} = |01\rangle\langle 10|_{i,j} \neq 0$, where the subscript i denotes action on the ith qubit. Thus, σ_i^- and σ_j^+ alone cannot replicate the anticommutation relations of the operators a_i , and a_j^\dagger .

The Jordan-Wigner transformation defines \mathbb{A}_i and \mathbb{A}_j^{\dagger} via

$$a_i \longmapsto \mathbb{A}_i = \left(\bigotimes_{k=1}^{i-1} \sigma_k^z\right) \sigma_i^-$$
 (9)

$$a_j^{\dagger} \longmapsto \mathbb{A}_j^{\dagger} = \left(\bigotimes_{k=1}^{i-1} \sigma_k^z\right) \sigma_j^+.$$
 (10)

Using the anticommutation relations $\{\sigma_i^{\pm}, \sigma_i^z\} = 0$, these operators preserve the fermionic algebra, as

$$\{\mathbf{A}_i, \mathbf{A}_j^{\dagger}\} = \{\sigma_i^-, \sigma_i^z\} \left(\bigotimes_{k=i+1}^{j-1} \sigma_k^z\right) \sigma_j^+ = 0 \tag{11}$$

where j > i, as is required of a fermion-qubit mapping.

In our work we confine our discussion to Jordan-Wigner type mappings, which exhibit a direct and intuitive correlation between fermions and qubits. The correlation is thus: A_i and A_j^{\dagger} naturally act on the spin basis $\{|l_1, l_2, \ldots, l_n\rangle \mid l_i \in \{0, 1\}\}$ in exactly the same way that the fermionic creation and annihilation operators a_i and a_j^{\dagger} act on the Fock basis $\{|j_1, j_2, \ldots, j_n\rangle \mid j_i \in \{0, 1\}\}$. That is, $l_i = j_i$. This is in contrast to other fermion-qubit mappings – for example in the case of the Bravyi-Kitaev

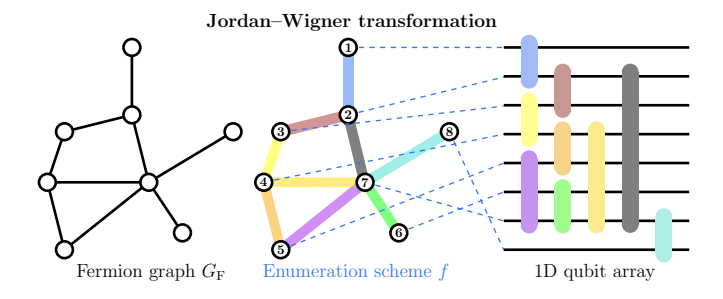


Figure 2: The Jordan-Wigner transformation converts an n-fermion Hamiltonian into strings of unitary Pauli gates on n qubits. Here, the graph $G_{\rm F}$ represents the single-fermion hopping interactions of the Hamiltonian.

transformation [26], the operators A_i and A_j^{\dagger} act on a basis for qubit space $\{|b_1, b_2, \dots, b_n\rangle \mid b_i \in \{0, 1\}\}$, where $b_i = \sum_k [\mathbf{B}]_{ik} j_k$ and \mathbf{B} is a specific invertible matrix.

D. Jordan-Wigner transformation of Hamiltonian hopping terms

Typical molecular electronic Hamiltonians H acting on n fermions have the form

$$H = \sum_{\alpha\beta} (h_{\alpha\beta}) a_{\alpha}^{\dagger} a_{\beta} + \frac{1}{2} \sum_{\alpha\beta\gamma\delta} (h_{\alpha\beta\gamma\delta}) a_{\alpha}^{\dagger} a_{\beta}^{\dagger} a_{\gamma} a_{\delta} , \quad (12)$$

where the indices $\alpha, \beta, \gamma, \delta$ are unordered labels for the n fermions. The complex coefficients $h_{\alpha\beta}$ and $h_{\alpha\beta\gamma\delta}$ are respectively one- and two-electron overlap integrals, such that H is Hermitian. The Hamiltonian in Equation 12 is an example of the Fermi-Hubbard model and conserves particle number. As the molecular system involves elec-

trons, which are spin- $\frac{1}{2}$ fermions, the indices in the summations both run through the different spin orbitals of each electron and also traverse over all of the electrons.

The Jordan-Wigner transformation uses a fermion enumeration scheme f to convert the indices $\alpha, \beta, \gamma, \delta$ into numerical indices $i, j, k, l \in \{1, 2, ..., n\}$. It then transforms the single-electron excitation terms of H, known as hopping terms, into strings of Pauli gates:

$$a_i^{\dagger} a_i \longmapsto \frac{1}{2} \left(\mathbb{1}_i - \sigma_i^z \right) = \frac{1}{2} \left(\mathbb{1}_i - Z_i \right)$$
 (13)

$$a_i^{\dagger} a_j \longmapsto \frac{1}{2} \left(X_i - Y_i \right) \left(\bigotimes_{k=-i}^{j-1} Z_k \right) \frac{1}{2} \left(X_j + Y_j \right) , \quad (14)$$

where i < j in Equation 14, and $Z = \sigma^z$. Figure 2 visualises how the Jordan-Wigner transformation maps the hopping terms in a fermionic system into Pauli strings. Here the fermions have a connectivity graph $G_{\rm F}$, which means the Hamiltonian only includes the hopping term $a_{\alpha}^{\dagger}a_{\beta}$ if (α, β) is an edge of $G_{\rm F}$.

After using an enumeration scheme for the fermions, Figure 3 demonstrates the transformation of hopping terms $a_2^{\dagger}a_7$ and $a_5^{\dagger}a_4$. However, these hopping terms would not feature in a Hamiltonian without appearing alongisde their complex conjugate terms.

Indeed, to ensure that H is Hermitian, in any Hamiltonian H the term $h_{ij}a_i^{\dagger}a_j$ will always appear alongside its conjugate term $(h_{ij})^*a_j^{\dagger}a_i$. Thus it is no less complete a description of the fermionic system to neglect Equation 14 and instead only consider Equation 15. In the case when the coefficients of the grouped terms are $h_{ij} = (h_{ij})^* = 1$, the transformation is simply Equation 16. Figure 4 illustrates the conversion of conjugate hopping terms of the form of Equation 16 into quantum circuits.

$$h_{ij}a_i^{\dagger}a_j + (h_{ij})^*a_j^{\dagger}a_i \longmapsto \frac{\operatorname{Re}(h_{ij})}{2} \left(\bigotimes_{k=i+1}^{j-1} Z_k\right) \left(X_i \otimes X_j - Y_i \otimes Y_j\right) + \frac{i\operatorname{Im}(h_{ij})}{2} \left(\bigotimes_{k=i+1}^{j-1} Z_k\right) \left(Y_i \otimes X_j - X_i \otimes Y_j\right). \tag{15}$$

$$a_i^{\dagger} a_j + a_j^{\dagger} a_i \longmapsto \frac{1}{2} \left(\bigotimes_{k=i+1}^{j-1} Z_k \right) \left(X_i \otimes X_j - Y_i \otimes Y_j \right).$$
 (16)

E. Complexity-theoretical preliminaries

This section introduces the necessary notation and complexity theoretic problems that underpin our results. A visual summary of the hierarchy of these problems appears in Figure 28. All problems start with some variation of the following ingredients:

1. A graph G = (V, E) with |V| = n vertices and

edge set $E \subseteq V \times V$, and

- 2. a weight function $w: E \to \mathbb{R}$ describing flows between vertices, and
- 3. a list L of possible **locations** for the vertices, and
- 4. a **distance function** $d: L \times L \to \mathbb{R}$ describing the spatial separation between the locations.

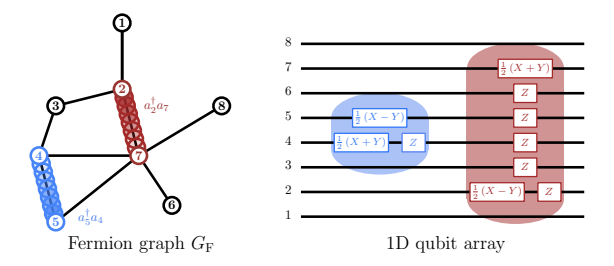


Figure 3: **Left:** representation of individual terms $a_2^{\dagger}a_7$ and $a_5^{\dagger}a_4$ in a fermionic Hamiltonian describing an unstructured system of fermions. **Right:** Jordan-Wigner transform of these terms into strings of Pauli operators acting on qubits.

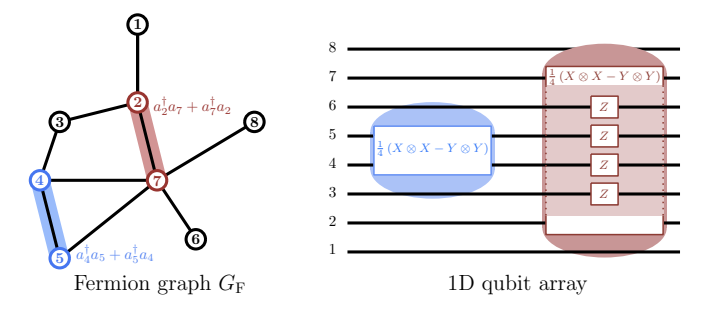


Figure 4: **Left:** as the Hamiltonian is Hermitian, every individual term of the form $a_i^{\dagger}a_j$ can pair with its Hermitian conjugate $a_j^{\dagger}a_i$. **Right:** Jordan-Wigner transform of the grouped terms $a_i^{\dagger}a_j + a_j^{\dagger}a_i$ into strings of Pauli operators acting on qubits.

This section lists graph problems relevant to the discussion in this paper. All problems have the objective of finding a surjective **assignment function** $f:V\to L$ to place the vertices in locations so as to minimise a cost function.

1. NP-hard problems

The following problem was shown by Koopmans [27] to be NP-hard:

QUADRATIC ASSIGNMENT

INSTANCE: Graph G=(V,E), weight function $w:E\to\mathbb{R}$, vertex locations L, distance function $d:L\times L\to\mathbb{R}$.

PROBLEM: Find the location assignment function $f: V \to L$ in such a way as to minimise the cost function

$$C(f) = \sum_{(\alpha,\beta)\in E} w(u,v) \cdot d(f(\alpha), f(\beta)) . \quad (17)$$

2. Problems that are at least NP-complete.

The following problems appear to generalise some NP-complete problems, however it is unknown if they are NP-complete themselves or if they are actually NP-hard.

The optimal linear arrangement problem was first studied by Garey and Johnson [22]. Note that it is different to the "optimal linear arrangement" in their book [24]. This is a special case of the quadratic assignment problem: the weight function w is restricted to integer values, the vertex locations L are $\{1,2,\ldots,n\}$, and the distance metric is d(i,j)=|i-j|. According to Horton [28], it is not known whether the optimal linear arrangement problem as written here is NP-hard or NP-complete.

OPTIMAL LINEAR ARRANGEMENT

INSTANCE: Graph G = (V, E), weight function $w : E \to \mathbb{Z}$.

PROBLEM: Find the enumeration scheme $f: V \to \{1, 2, ..., n\}$ that minimises the cost function

$$C(f) = \sum_{(\alpha,\beta)\in E} w(\alpha,\beta) \cdot |f(\alpha) - f(\beta)| . \quad (18)$$

The minimum p-sum problem was studied by Mitchison and Durbin [21], Garey and Johnson [23], and Juvan and Mohar [29]. It is a special case of the optimal linear arrangement problem: its weight function is effectively $w(\alpha,\beta)=|f(\alpha)-f(\beta)|^{p-1}\in\mathbb{Z}$. This problem is NP-complete for p=1 [22], p=2 [30] and $p\to\infty$ [28]. One could also consider the broader class of problems where $p\in\mathbb{R}^+$, as done by Mitchison and Durbin [21]. These problems are likely to be at least as hard as their integer-p equivalents.

MINIMUM p-SUM

INSTANCE: Graph G = (V, E), integer $p \in \mathbb{Z}$. **PROBLEM**: Find the enumeration scheme $f : V \to \{1, 2, \dots, n\}$ that minimises the cost function

$$C^{p}(f) = \left(\sum_{(\alpha,\beta)\in E} |f(\alpha) - f(\beta)|^{p}\right)^{1/p}.$$
 (19)

3. NP-complete problems.

The following problem was introduced in [22]:

EDGESUM (or SIMPLE OPTIMAL LINEAR ARRANGEMENT, MINIMUM 1-SUM)

INSTANCE: Graph G = (V, E).

PROBLEM: Find the enumeration scheme $f: V \to \{1, 2, \dots, n\}$ that minimises the cost function

$$C(f) = \sum_{(\alpha,\beta)\in E} |f(\alpha) - f(\beta)|. \qquad (20)$$

Figure 5 surveys the graphs with known solutions, as of the date of publication of Hortons's PhD thesis [28] which cites a solution for outerplanar graphs by Frederickson and Hambrusch [32]. Other sources include a survey by Lai [31], and solution for tree graphs by Chung [33]. This problem is known to be NP-complete via a reduction to the simple max-cut problem [22].

As an example of a comparable problem, consider the following:

BANDWIDTH (or MINIMUM ∞-SUM)

INSTANCE: Graph G = (V, E).

PROBLEM: Find the enumeration scheme $f: V \to \{1, 2, \dots, n\}$ that minimises the cost function

$$\max_{(\alpha,\beta)\in E} |f(\alpha) - f(\beta)| . \tag{21}$$

This is the minimum p-sum problem as $p \to \infty$. If G is an arbitrary tree graph, it is an NP–complete problem to solve the bandwidth problem for G [23]. In fact, Saxe proves that the decision problem as to whether the bandwidth is less than or equal to k = O(1) is efficiently solvable [34].

III. FERMION ENUMERATION SCHEMES AND QUANTUM CIRCUIT COST

In this section, we only consider Jordan-Wigner transformations from n-fermion to linear n-qubit systems. However, recent works such as the Verstraete-Cirac [12] and Steudtner-Wehner mappings [16] use m>n qubits with square-lattice connectivity. We design a novel mapping with m=n+2 qubits in Section IV, and we argue in Section V B that the optimality results of this section are beneficial in qubit systems with any connectivity.

A. Enumeration schemes and figures of merit

Given an n-fermion system with a Hamiltonian H, the first step of any Jordan-Wigner process is always to label the fermions with an enumeration scheme f. The

hopping term $a_{\alpha}^{\dagger}a_{\beta}$ between fermions α and β is then $a_{f(\alpha)}^{\dagger}a_{f(\beta)}=a_{i}^{\dagger}a_{j}$. The Jordan-Wigner transform maps $a_{i}^{\dagger}a_{j}$ to Pauli strings on the 1D qubit array. Any given enumeration scheme f thus generates a unique list of Pauli strings. Figure 7 gives three examples.

We propose the strategy of choosing a fermion enumeration scheme that minimises a property of its induced list of Pauli strings. This property should pertain to the efficiency of the quantum computer, be it depth, gate count, or some other measure. We define several such properties below.

1. Average Pauli weight. The Pauli weight of a string of Pauli operations is the number of qubits involved in the string. A natural property to try and minimise by choosing an enumeration sscheme f is the average weight of all the Pauli strings that the corresponding Jordan-Wigner transform produces. This corresponds to minimising the objective function

$$C^{1}(f) := \sum_{(\alpha,\beta) \in G_{F}} |f(\alpha) - f(\beta)|.$$
 (22)

For a given fermion connectivity graph G_F , the formula for the average Pauli weight of enumeration f (denoted as APV(f)) is

$$APV(f) := \frac{C^1(f)}{|G_F|} + 1,$$
 (23)

where $|G_{\rm F}|$ is the number of edges in $G_{\rm F}$. The extra term of 1 accounts for the fact that the weight of a Pauli string between qubits with labels i and j is |i-j|+1. Figure 7 shows the average Pauli weight on the 6×6 lattice for three enumeration schemes: the S-pattern $f_{\rm S}$, the Z-pattern $f_{\rm Z}$, and the Mitchison-Durbin pattern, $f_{\rm M}$.

The search for such an enumeration scheme is an example of the NP-complete edgesum problem from Section II E. In Section III B, we present Theorem 1 for an enumeration scheme $f_{\rm M}$ that minimises the average Pauli weight of a Jordan-Wigner mapping if $G_{\rm F}$ is the square lattice. Through Corollary 1.1, this lends an improvement to existing protocols for square lattice fermion simulation by reducing the average Pauli weight by up to $\approx 13.9\%$.

2. Average pth power of Pauli weight. One might want to optimise the locality of the qubit interactions, which the average pth power of the Pauli weights quantifies, where $p \in \mathbb{R}^+$. Minimising this property corresponds to finding the enumeration scheme f that minimises the objective function

$$C^{p}(f) := \left(\sum_{(\alpha,\beta) \in G_{\mathcal{F}}} |f(\alpha) - f(\beta)|^{p}\right)^{1/p}.$$
 (24)

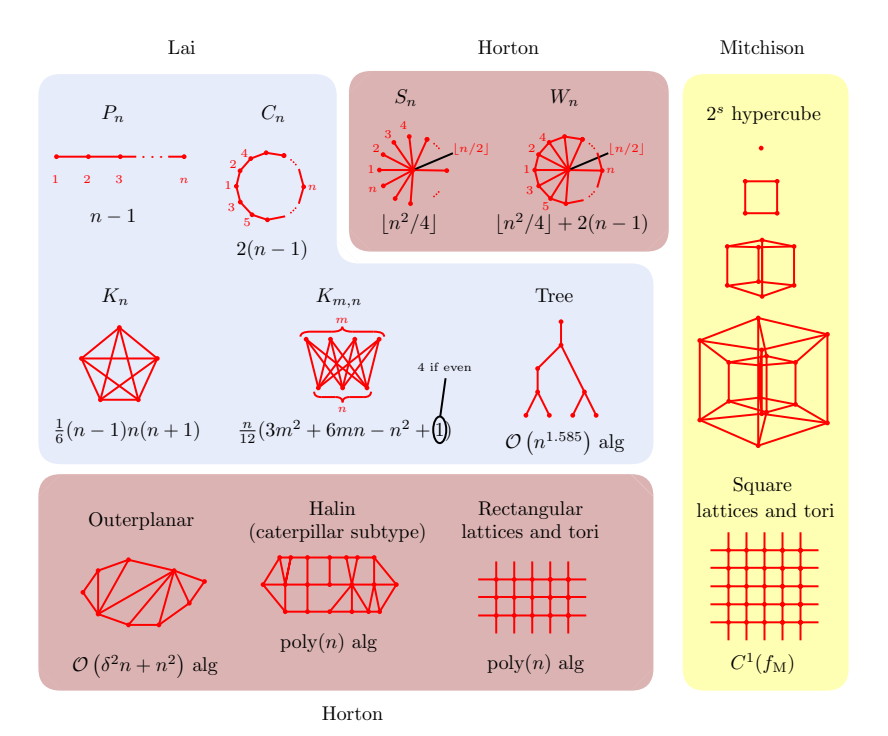


Figure 5: Graph families with known solutions to their edgesum problems. The formula for the minimum edgesum appears beneath each graph's image, if it exists, or the cost of the best-known classical algorithm for solving that graph's edgesum problem if not. References for the solution of these graphs appear in Lai [31], Horton [28], and Mitchison's [21] works as indicated.

In Section III E, we present numerical results for the minimum p-sum problem to illustrate how one might choose fermion enumeration schemes to optimise over this objective function.

- 3. Depth of circuit implementing of all Pauli strings. In contrast to the above, another way to quantify the effectiveness of the enumeration scheme is the smallest number of timesteps in which a quantum circuit might implement all Pauli strings. Figure 8 shows quantum circuits implementing all hopping terms on the 6×6 lattice for $f_{\rm S}, f_{\rm Z}$, and $f_{\rm M}$, along with the depths of these circuits.
- 4. Other properties. One may also consider other properties. For example, if the qubits have a connectivity graph $G_{\mathbf{Q}}$, it may be desirable to make the Pauli strings as local as possible on $G_{\mathbf{Q}}$. We include a discussion of this optimization in Section V B.

B. Minimising the average Pauli weight for a square fermionic lattice

We will now exhibit an optimal fermion-qubit mapping – one that minimises the average Pauli weight. It turns out that the most efficient way to label fermions is related

to the work of Graeme Mitchison and Richard Durbin when they studied the organisation of nerve cells in the brain cortex [21]. Figure 6 displays the pattern, which is dramatically different to the S-pattern and its variations [12, 16]. The proof of our main result below makes use of this curious arrangement to construct a fermion-qubit mapping with optimal $C^1(f)$ locality.

Theorem 1. (Minimising the average Pauli weight of the Jordan-Wigner mapping for the n-fermion square lattice.) Given a system of $n = N^2$ fermions interacting in a square $N \times N$ lattice G_F , then the Mitchison-Durbin pattern f_M is a fermion enumeration scheme that minimises the average Pauli weight of the hopping terms.

Proof. Proof in Section III C. \square

Remark 1. Optimising the average Pauli weight depends on the edgesum value $C^1(f)$, therefore calculating the optimal fermion enumeration scheme for an arbitrary fermion graph $G_{\rm F}$ is NP-complete as discussed in Section II E.

Remark 2 details all known scenarios to date where the optimal fermion enumeration scheme is solvable in $\mathsf{poly}(n)$ time.

Remark 2. (Solutions for other graph types $G_{\rm F}$.) If the Hamiltonian H is as defined in Theorem 1, and if $G_{\rm F}$ belongs to any of the graph families in Figure 5, then a

OPTIMAL NUMBERINGS OF AN N×N ARRAY*

GRAEME MITCHISON† AND RICHARD DURBIN†

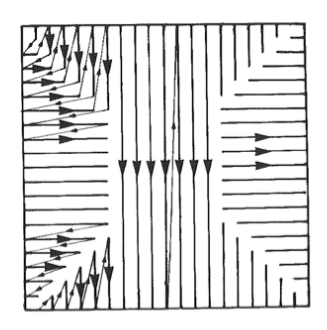




Figure 6: The original appearance of the Mitchison-Durbin pattern in their original paper [21], and Graeme Mitchison's sculpture of the optimal numbering of a 7×7 array. Reproduced with the permission of Richard Durbin.

classical computer can efficiently find an optimal fermion enumeration scheme for H.

Corollary 1.1. Using the Mitchison-Durbin pattern $f_{\rm M}$ to enumerate a square-lattice fermionic system produces Pauli strings with an average weight of $\frac{1}{3} \left(4 - \sqrt{2}\right) \approx 0.86$ times the corresponding average Pauli weight that the S-pattern $f_{\rm S}$ produces. That is, quantum circuits to implement the lattice hopping terms are shorter by 13.9%.

Proof. On an $N\times N$ lattice, the Mitchison-Durbin pattern $f_{\rm M}$ and the S–pattern $f_{\rm S}$ have edgesums

$$C^{1}(f_{S}) = N^{3} - N \tag{25}$$

$$C^{1}(f_{\rm M}) = N^{3} - xN^{2} + 2x^{2}N - \frac{2}{3}x^{3} + N^{2}$$

$$- xN - 2N + \frac{2}{3}x,$$
(26)

respectively. In Equation 26, the value x is the closest integer to $N-\frac{1}{2}\sqrt{2N^2-2N+\frac{4}{3}}$ (proof in Section III C1). By inspection, $C^1(f_{\rm S})>C^1(f_{\rm M})$ for $N\geq 6$. With computer assistance it is straightforward to calculate the limit of the ratio of the two patterns' edgesums:

$$\lim_{N \to \infty} \frac{C^1(f_{\rm M})}{C^1(f_{\rm S})} = \frac{4 - \sqrt{2}}{3} \approx 0.86.$$
 (27)

In terms of the resource savings in designing a quantum computer, using Equation 23 the average Pauli weights approach the same limit:

$$\lim_{N \to \infty} \left(\left(\frac{C^{1}(f_{\rm M})}{2N(N-1)} + 1 \right) \left(\frac{C^{1}(f_{\rm S})}{2N(N-1)} + 1 \right)^{-1} \right)$$

$$= \lim_{N \to \infty} \frac{C^{1}(f_{\rm M})}{C^{1}(f_{\rm S})} = \frac{4 - \sqrt{2}}{3} \approx 0.86.$$
 (28)

We can conclude from Corollary 1.1 that a quantum computer simulation of a square fermionic Hamiltonian could save over 13.9% on quantum gate resources simply by labelling the fermions using the Mitchison-Durbin pattern rather than the S-pattern. Even in the case of simulating small fermionic systems, this method provides a worthwhile advantage. For example, in Figure 7 where N=6, the ratio of the average Pauli weights using $f_{\rm M}$ and $f_{\rm S}$ is $4.33/4.5\approx 0.96$. That is, even for the 6×6 lattice, applying Theorem 1 could reduce quantum circuit size by 4%.

For $2 \leq N \leq 20$, Figure 9 shows the resulting average Pauli weights of various enumeration schemes on $N \times N$ lattices. For N=20, $C^1(f_{\rm M})/C^1(f_{\rm S})=\frac{7140}{7980}\approx 89.5\%$. Even on lattices of these restricted sizes, the Mitchison-Durbin pattern can yield a reduction of over 10% from that of the S–pattern.

C. Proof of Theorem 1

This section contains a more elaborate version of the original proof [21]. The Mitchison-Durbin pattern $f_{\rm M}$ solves the edgesum or minimum 1-sum problem for an $N\times N$ lattice. Thus, its optimality (once proved) directly implies that the pattern $f_{\rm M}$ is an optimal choice to minimise the average Pauli weight of a Jordan-Wigner mapping, and Theorem 1 follows as a consequence.

Let G = (V, E) be the $N \times N$ square lattice. Label each vertex $\alpha \in V$ by its position (μ, ν) on the lattice, where $\mu, \nu \in \{1, 2, \dots, N\}$. For example, the vertex in the top-left corner has label (1, 1) and the vertex in the bottom-right has label (N, N).

Fermion enumeration schemes for the 2D lattice

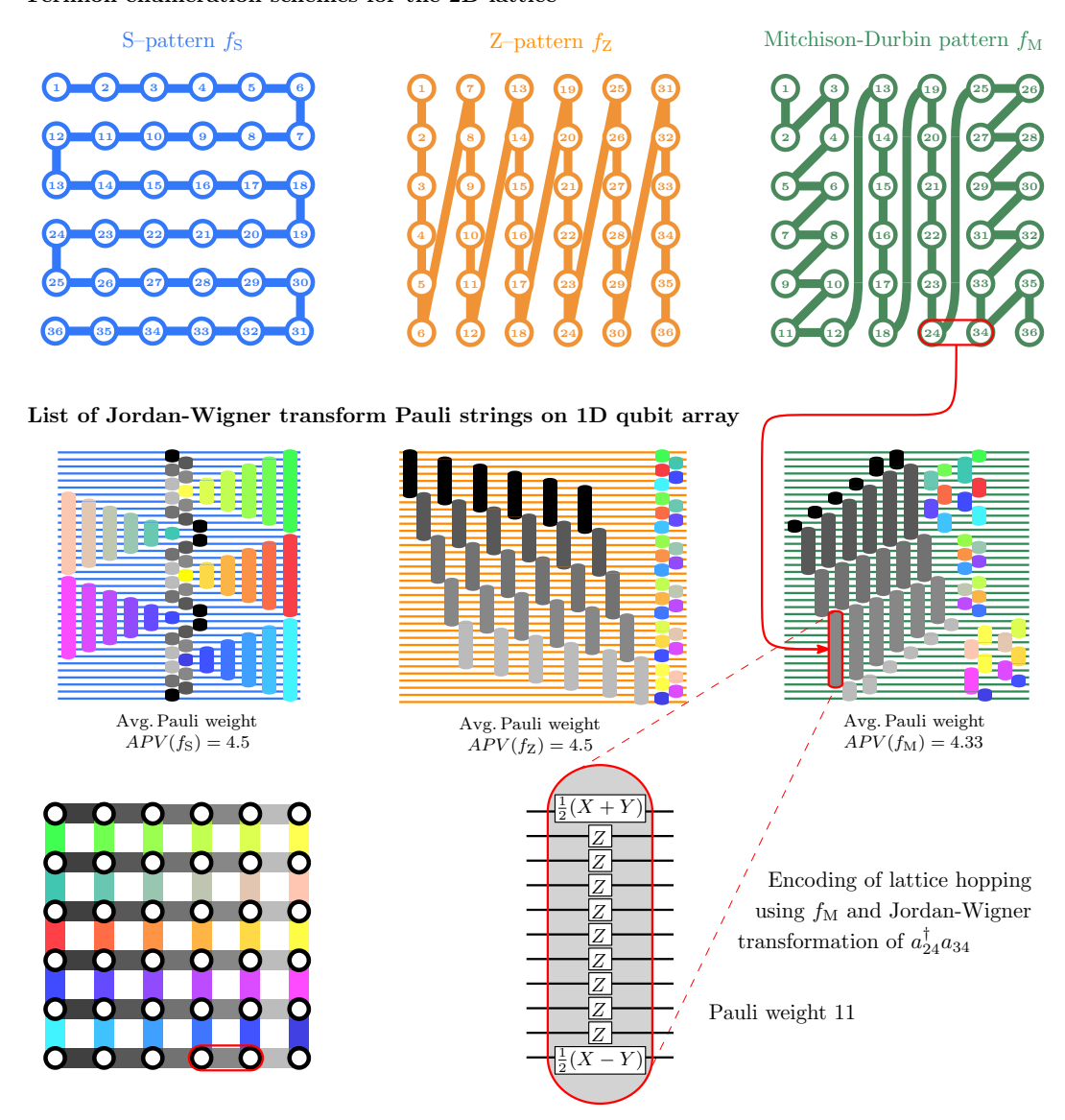


Figure 7: Three different enumeration schemes for the 6×6 lattice of fermions and the Pauli strings they produce. Pauli strings correspond to the hopping term of the same colour in the 6×6 lattice in the bottom left of the figure. On square lattices, the Mitchison-Durbin pattern produces Pauli strings of the lowest average weight.

Given a square lattice vertex enumeration scheme $f:V\to\{1,2,\ldots,N^2\}$, the cost function for the minimum p-sum problem is then

$$(C^{p}(f))^{p} = \sum_{(\alpha,\beta)\in E} |f(\alpha) - f(\beta)|^{p}$$
(29)

$$= \sum_{(\mu,\nu)\in V} \left(\underbrace{\left| f(\mu+1,\nu) - f(\mu,\nu) \right|^p}_{\text{horizontal; 0 if } (\mu+1,\nu)\notin V} \right)$$
(30)

$$+\underbrace{\left|f(\mu,\nu+1)-f(\mu,\nu)\right|^p}_{\text{vertical; 0 if }(\mu,\nu+1)\notin V}\right).$$

Call an enumeration scheme f for the square lattice G

horizontally ordered if $f(\mu, \nu+1) > f(\mu, \nu)$ for all vertices $(\mu, \nu) \in V$. Similarly, call f vertically ordered if $f(\mu + 1, \nu) > f(\mu, \nu)$ for all $(\mu, \nu) \in V$.

Proposition 1. Let $p \ge 1$. Given a vertex enumeration scheme $f: V \to \{1, 2, \dots, N^2\}$ for the $N \times N$ square lattice, then there exists a horizontally and vertically ordered enumeration scheme g such that $C^p(g) \le C^p(f)$. That is, there exists an optimal enumeration scheme for the $N \times N$ square lattice which is horizontally and vertically ordered.

Proof. Let f be a vertex enumeration scheme for the square lattice. Consider the enumeration scheme f' which is horizontally ordered, but otherwise the same

Minimum depth of all Pauli strings

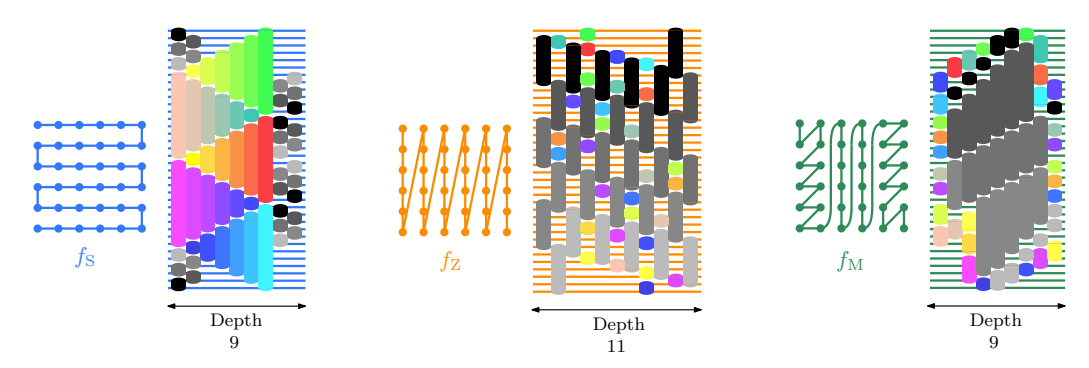


Figure 8: Comparison of the "parallelisability" of Pauli strings produced by three different enumeration schemes on a 6×6 square lattice of fermions. The unit of merit is the depth of a quantum circuit implementing all Pauli strings. Pauli strings correspond to hopping terms of the same colour in the lattice in Figure 7.

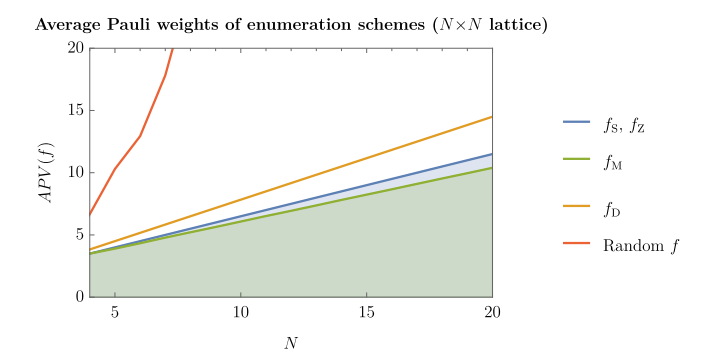


Figure 9: The average Pauli weights APV(f) of various enumeration schemes on $N \times N$ lattices. Random f is a randomly-generated enumeration scheme in this instance.

as f. Thus, each row of the enumerated lattice f'(G) contains the same set of indices as f(G), except that the indices are permuted so as to be in order of ascending value if they were not already. Call the process of replacing f with f' the horizontal ordering of f. Define the vertical ordering of f similarly. We will prove Proposition 1 via successively proving statements S1–S3 below:

S1. The action of horizontally ordering an enumeration scheme f never increases $C^p(f)$.

The following two claims prove S1:

<u>Claim</u>: The horizontal ordering of f will always decrease the horizontal contributions to $C^p(f)$ in Equation 30 if $p \ge 1$.

<u>Proof:</u> Suppose f is not horizontally ordered; for example, there may be a row of the enumerated lattice f(G) such as the one in the top diagram of Figure 10. The horizontal contributions to $C^p(f)$

from this row are

$$|j_{1} - j_{2}|^{p} + |j_{2} - j_{3}|^{p} + |j_{3} - j_{4}|^{p} + \dots + |j_{i-1} - j_{i}|^{p} + |j_{i} - j_{i+1}|^{p} + \dots + |j_{N-1} - j_{N}|^{p}.$$
(31)

Consider modifying f by rearranging the positions of j_{i+1} and j_i , as in the second diagram of Figure 10. The contributions to $C^p(f)$ would now be:

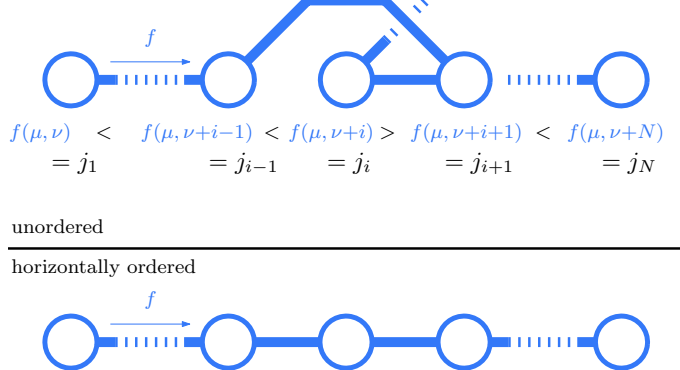
$$|j_{1} - j_{2}|^{p} + |j_{2} - j_{3}|^{p} + |j_{3} - j_{4}|^{p} + \dots + |j_{i-1} - j_{i+1}|^{p} + |j_{i+1} - j_{i}|^{p} + \dots + |j_{N-1} - j_{N}|^{p}.$$
(32)

The difference in the horizontal contribution to $C^p(f)$ upon modifying f in this way is thus the difference between Equations 32 and 31. This value is $|j_{i-1} - j_{i+1}|^p - |j_{i-1} - j_i|^p < 0$ if $p \ge 1$ because $j_{i+1} < j_i$.

The action of horizontally ordering f is simply a chain of as many swaps of the above form as is necessary to leave the vertices in each row of the lattice in ascending order. Thus, horizontally ordering f will always decrease the horizontal contributions to $C^p(f)$ if $p \geq 1$.

<u>Claim</u>: The horizontal ordering of f will never increase the vertical contributions to $C^p(f)$ in Equation 30 if $p \ge 1$.

<u>Proof:</u> (Use Figure 11 as a guide.) Suppose that f is not horizontally ordered. Vertical contributions to $C^p(f)$ will change upon the horizontal ordering of f if the process affects adjacent rows differently. This occurs if there exist vertices (μ, ν) and $(\mu, \nu + 1)$ which are horizontally ordered with $f(\mu, \nu) = i < f(\mu, \nu + 1) = j$, and if vertices $(\mu + 1, \nu)$ and $(\mu + 1, \nu + 1)$ are not, with $f(\mu + 1, \nu) = m > f(\mu + 1, \nu + 1) = n$.



 $f(\mu,\nu) < f(\mu,\nu+i-1) < f(\mu,\nu+i) < f(\mu,\nu+i+1) < f(\mu,\nu+N) = j_1 = j_{i-1} = j_i = j_N$

Figure 10: On a square lattice graph, horizontally ordering each row never increases the edgesum.

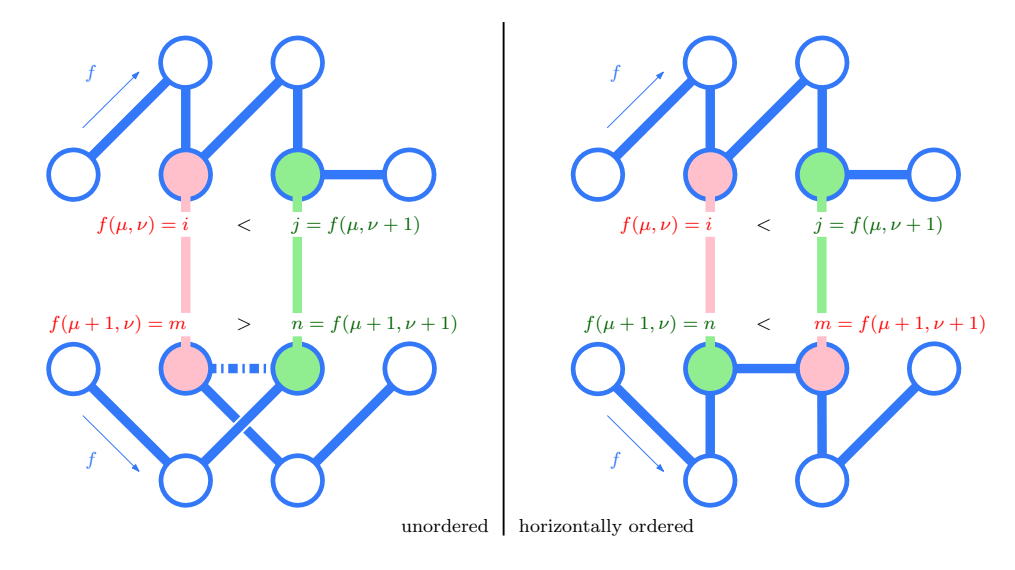


Figure 11: On a square lattice graph, the action of horizontally ordering a vertex enumeration scheme f never increases the vertical contributions to $C^p(f)$.

Initially, the vertical contributions to $C^p(f)$ from these four vertices is

$$|i - m|^p + |j - n|^p$$
. (33)

Because i < j and m > n, the values (i - m) and (j - n) in Equation 33 are unequal. Consider modifying f by rearranging the positions of m and n, as in Figure 11. The new vertical contributions are

$$|i-n|^p + |j-m|^p$$
. (34)

The values of (i-n) and (j-m) may not be equal, but they are closer in value to each other than the values (i-m) and (j-n) were. For p>1, if a+b is constant then a^p+b^p reduces in value the closer a and b are to each other. Therefore, the vertical contributions to $C^p(f)$ in Equation 34 are less than the vertical contributions in Equation 33.

If p = 1, the contributions are unchanged by the modification. This proves the claim.

S2. The action of vertically ordering a horizontally ordered enumeration scheme f preserves its horizontal ordering.

Suppose that f is a horizontally ordered enumeration scheme. This claim proves S2:

<u>Claim:</u> The vertical ordering of f preserves the horizontal ordering.

<u>Proof:</u> (Use Figure 12 as a guide.) Let g be the vertically ordered version of f, and suppose that it is not horizontally ordered. Then there must be a pair of vertices (μ, ν) and $(\mu, \nu') \in V$ in the lattice such that $g(\mu, \nu) = k < g(\mu, \nu')$ and $\nu' < \nu$, for $k \in \{1, 2, \dots, N^2\}$.

The enumeration scheme g is vertically ordered: therefore, each of the $\mu-1$ vertices above (μ,ν)

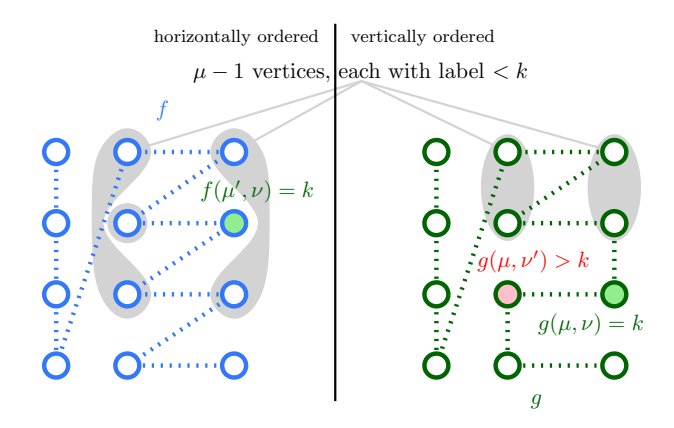


Figure 12: If a vertex enumeration scheme f is horizontally ordered, then its vertical ordering g must also be horizontally ordered. This figure shows the contradiction that would arise if this were not the case.

must have a value less than $g(\mu, \nu) = k$. Because the vertex with label k is on the same row as (μ', ν) , then each of the $\mu - 1$ vertices above (μ, ν') must also have a value less than k.

Now consider the original enumeration scheme f, before vertical ordering. The vertex with label k is in the same column of the lattice as it was under g, i.e. column ν . Let this vertex be (μ', ν) ; then $f(\mu', \nu) = k$. Because g is just a vertical ordering of f, there must still be $\mu - 1$ vertices in columns ν and ν' with label less than k, and because f is horizontally ordered then every vertex to the left of these $\mu - 1$ vertices has a label with value less than k. But every vertex to the left of (μ', ν) must also have a label with value less than k, as $f(\mu', \nu) = k$. Therefore, under the enumeration scheme f, any column to the left of column ν contains $(\mu - 1)$ + $1 = \mu$ vertices with labels of value less than k. But we know that column ν' contains exactly $\mu-1$ vertices with label less than k, and $\nu' < \nu$. This is a contradiction.

S3. For every vertex enumeration scheme f there exists a horizontally and vertically ordered scheme g with $C^p(g) \leq C^p(f)$.

This results from combining statements S1 and S2.

This proves Proposition 1. \Box

Proposition 1 informs the discussion of numeric results when p > 1 in Section III E. However, from this point the proof of Theorem 1 only concerns the minimum 1-sum problem, for which p = 1. Every enumeration scheme referenced from hereon is horizontally and vertically ordered. The following result greatly simplifies the calculation of $C^1(f)$:

<u>Claim:</u> Let V_l , V_r , V_t , V_b be the vertices in the left column, right column, top row and bottom row of the square lat-

tice, respectively. Given a horizontally and vertically ordered vertex enumeration scheme $f:V\to\{1,2,\ldots,N^2\}$ for the lattice, the cost function for the minimum 1-sum problem is

$$C^{1}(f) = \sum_{\alpha \in V_{b}} f(\alpha) + \sum_{\alpha \in V_{r}} f(\alpha) - \sum_{\alpha \in V_{l}} f(\alpha) - \sum_{\alpha \in V_{t}} f(\alpha).$$
(35)

<u>Proof:</u> As f is horizontally and vertically ordered, Equation 30 becomes

$$C^{1}(f) = \sum_{(\mu,\nu)\in V} \left(f(\mu+1,\nu) + f(\mu,\nu+1) - 2f(\mu,\nu) \right)$$
(36)

$$= 2f(N,N) + \sum_{\mu=2}^{N-1} f(\mu,N) + \sum_{\nu=2}^{N-1} f(N,\nu)$$
(37)
$$- \sum_{\mu=2}^{N-1} f(\mu,1) - \sum_{\nu=2}^{N-1} f(1,\nu) - 2f(1,1)$$

$$= \sum_{\alpha \in V_{b}} f(\alpha) + \sum_{\alpha \in V_{r}} f(\alpha) - \sum_{\alpha \in V_{l}} f(\alpha) - \sum_{\alpha \in V_{t}} f(\alpha) .$$
(38)

Any horizontally and vertically ordered enumeration scheme f must begin at a corner of the square lattice and end at the opposite corner. Assume without loss of generality that f(1,1)=1 and $f(N,N)=N^2$, and that f(N,1)< f(1,N). As in Figure 13, let U be the section of the lattice that f labels up to (N,1), and let V be the section of the lattice that it labels from (1,N) onwards. Because f can never "double back" on itself without violating horizontal or vertical ordering, the regions U and V are upper- and lower- skew block-triangular sections of the lattice, respectively.

Define S(U) and S(V) to be the sums of the labels of vertices on the boundary of the lattice in the regions U and V, respectively. By Equation 35, these S quantities completely determine the contributions to $C^1(f)$ from the vertices in U and V. Suppose that U and V are fixed regions, and that the goal is to choose an enumeration scheme f to maximise S(U) and minimise S(V). Lemma 2 provides a strategy to solve this problem.

Lemma 2. Let U and V be upper- and lower- skew block-triangular regions of the $N \times N$ square lattice, containing vertices (N,1) and (1,N) respectively, as above. For any enumeration scheme $f:V \to \{1,2,\ldots,N^2\}$ that labels the vertices in U before any outside of U, and labels the vertices in V after any outside of V, define S(U) and S(V) to be the sums of the labels on the lattice boundaries of U and V, respectively. Then, the rules below construct a horizontally and vertically ordered enumeration scheme f that yields the maximum value for S(U):

a) Fill each new column/row as far as possible while preserving horizontal and vertical ordering;

b) After filling a column/row as far as possible, begin to fill the longest remaining column/row that remains, starting from the top-leftmost available vertex of the lattice.

By symmetry, the reverse of this process provides a scheme that yields the minimum value for S(V).

Proof. (For reference, Figure 13 provides one example each of ordered enumeration schemes that do and do not satisfy the rules in Lemma 2.)

For a): if f did not fill a row as far as possible, then the first label on the subsequent column would be less than if f had filled the initial row, as Figure 14 demonstrates. Only the first entries of each row and column contributing to S(U), so this is not an optimal result.

For b): suppose that, beginning at index i, the enumeration scheme f fills a column of length a before it fills a row of length b > a, as in Figure 15. Then the contribution of the row and column to S(U) is i+(i+a). However, following rule b) in Lemma 2 would mean filling the row before the column, and the contribution to S(U) would be i+(i+b)>i+(i+a). Therefore, optimal enumeration schemes must follow rule b) as well as rule a).

Note that rules a) and b) describe a unique enumeration scheme for U, and so it is not possible to prescribe any further rules. Thus the resulting enumeration scheme must maximise S(U).

Corollary 2.1. The consequence of the rules in Lemma 2 is that an enumeration scheme f that minimises $C^1(f)$ must:

- a) Fill the largest square that lies in U by alternating between successively longer rows and columns, before filling the remaining columns and rows of U that are outside the square in order of decreasing length (a detail that the rightmost diagrams in Figures 13 and 15 include);
- b) Fill $\overline{U \cap V}$, the region between U and V, with columns from top-to-bottom. This ensures that labels with the least possible value occupy the bottom row of the lattice outside V, and that labels with the greatest possible value occupy the top row of the lattice outside U.

<u>Proof:</u> Given Lemma 2, Corollary 2.1 is self-evident. Figure 13 illustrates Corollary 2.1 b). ■

Lemma 2 showed how to minimise C(f) for fixed shapes of the regions U and V; Lemmas 3 and 4 will show which shapes of U and V can give a global minimum for $C^1(f)$.

Lemma 3. Let U and V be regions of the $N \times N$ square lattice that satisfy Lemma 2's conditions, and let f be an optimal enumeration scheme that follows the rules of Lemma 2. Then, delete from U the region to the right of the largest square in U, and add it to $\overline{U} \cap \overline{V}$. Similarly,

delete from V the region to the left of the largest square in V, and add it to $\overline{U \cap V}$. This reduces $C^1(f)$.

Proof. Define E_1 to be sum of the labels of the topmost vertices in U that are to the right of the largest square in U, E_2 to be the sum of the labels of the leftmost vertices beneath the largest square in U, and E_3 to be the sum of the labels of the topmost vertices outside of U. Define F_1 , F_2 and F_3 analogously, as in Figure 16. Then,

$$C^{1}(f) = (F_1 + F_2 + F_3) - (E_1 + E_2 + E_3)$$
 (39)
+ labels of edge vertices in squares.

Any horizontally and vertically ordered enumeration scheme that follows the rules of Lemma 2 must label the vertices in the largest squares of U and V first and last. Therefore, the deletion operation in Lemma 3's statement does not change the labels of the edge vertices in the squares.

<u>Claim</u>: The deletion operation in Lemma 3 increases $(E_1 + E_2 + E_3)$.

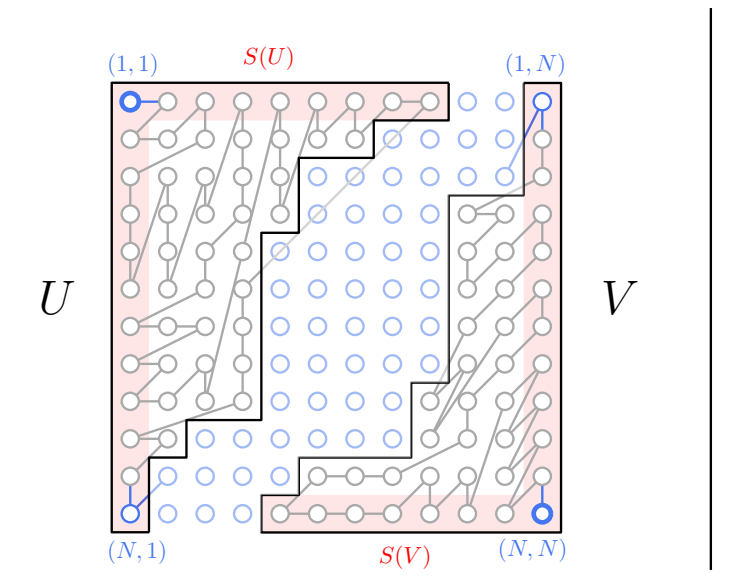
<u>Proof:</u> The following three steps implement the deletion operation in Lemma 3.

- 1. Delete from V the region to the left of the largest square in V, and add it to $\overline{U \cap V}$. This increases E_3 and leaves E_1 and E_2 unchanged.
- Delete the rightmost column from U, and add it to U∩V. As in Figure 17, let x be the side length of the largest square in U, let w be the height of the rightmost column of U and let h be the height of the bottommost row of U with length greater than w. This step reduces the labels of the bottommost h elements in E₂ by w, and so E₂ decreases by hw. Meanwhile, the value of E₁ increases because of the new label for the topmost vertex of the column that has joined U∩V. The label of this vertex increases by at least hx, and so the value of E₁+E₂ increases by hx hw = h(x w) > 0, as x > w.
- 3. Repeat step 2 until the entire region in U to the right of the largest square in U has joined $\overline{U \cap V}$. Breaking down the deletion operation in this way reveals that $E_1 + E_2 + E_3$ increases.

By symmetry, the deletion operation must therefore decrease $F_1+F_2+F_3$, and so $C^1(f)$ decreases overall. \square

Lemma 4 shows how to structure the regions outside the largest squares in U and V to give the least value for $C^1(f)$.

Lemma 4. Let U and V be regions of the $N \times N$ square lattice that satisfy Lemma 3's conditions, and let f be an optimal enumeration scheme that follows the rules of Lemma 2. Suppose the side length of the largest square in U is x. Then, modify U by imposing a length of x on all rows down to a height x above the bottom row, and



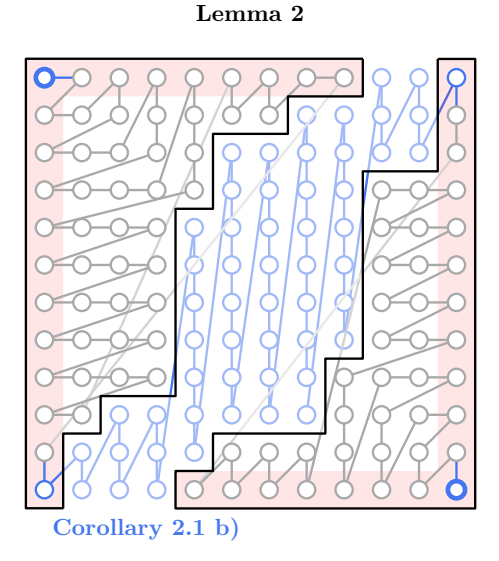


Figure 13: **Left:** An example of the regions U and V, and an ordered enumeration scheme that does not follow the rules in Lemma 2. Vertices on the boundaries of U and V contribute to S(U) and S(V). **Right:** An example of an enumeration scheme that follows the rules in Lemma 2 and hence maximises S(U) and minimises S(V). The scheme fills the space between U and V with vertical columns as a consequence, via Corollary 2.1 b).

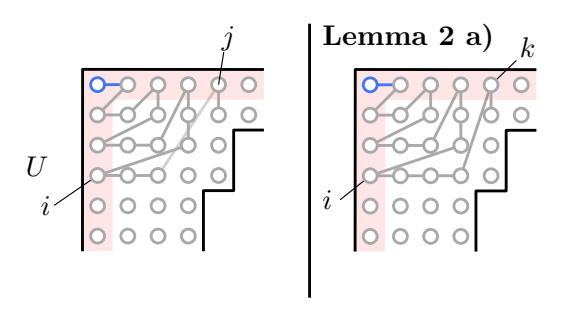


Figure 14: **Left:** An enumeration scheme that does not fill the row containing label i as far as possible. **Right:** The enumeration scheme now fills the row containing i as far as possible whilst preserving horizontal and vertical ordering. It is clear that k > j.

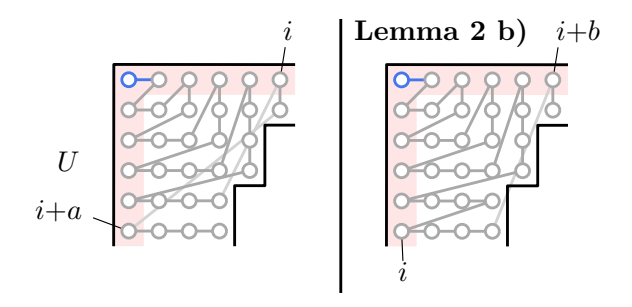


Figure 15: **Left:** An enumeration scheme that does not fill rows and columns in order of decreasing length. **Right:** The enumeration scheme now fills the row of length b before the column of length a < b. It is clear that i + (i + b) > i + (i + a).

then give the row at height y < x a length of y or y - 1. Perform the inverse modification to V.

For fixed x, the resulting optimal enumeration scheme with these new U and V yields the minimum $C^1(f)$ over all possible enumeration schemes for the square lattice.

Proof. As in Figure 19, take a row of U outside of the top-left square. Let it be the yth row from the bottom, and let its length be w. Then, if w < y, increase the row's length to w+1. This increases by +1 the labels of the y-1 bottommost vertices in the left-hand column of the lattice. Similarly, the labels of the w leftmost vertices in the bottom row increase by +1. With this modification to the enumeration scheme f, the value of $C^1(f)$ changes by $w-(y-1) \le 0$, i.e. it decreases by $(y-1)-w \ge 0$.

If w>y, decrease the row's length to w-1. This subtracts 1 from the labels of the y-1 bottommost vertices in the left-hand column of the lattice, and from the labels of the w-1 leftmost vertices in the bottom row. Thus the value of $C^1(f)$ changes by $-((w-1)-(y-1)) \leq 0$, i.e. it decreases by $w-y \geq 0$.

By symmetry, the inverse process works on V. Repeated application of these steps thus minimises $C^1(f)$; Figure 18 shows the end result.

Finally, only one degree of freedom remains in choosing the shape of U: the side length x of its largest square. Lemma 5 expresses the edgesum of the pattern as a function of N and x. Corollary 5.1 then provides the optimal value for x and hence the Mitchison-Durbin pattern $f_{\rm M}$

Lemma 5. Let U and V be regions of the $N \times N$ square lattice that satisfy Lemma 4's conditions, and let f be an optimal enumeration scheme that follows the rules of

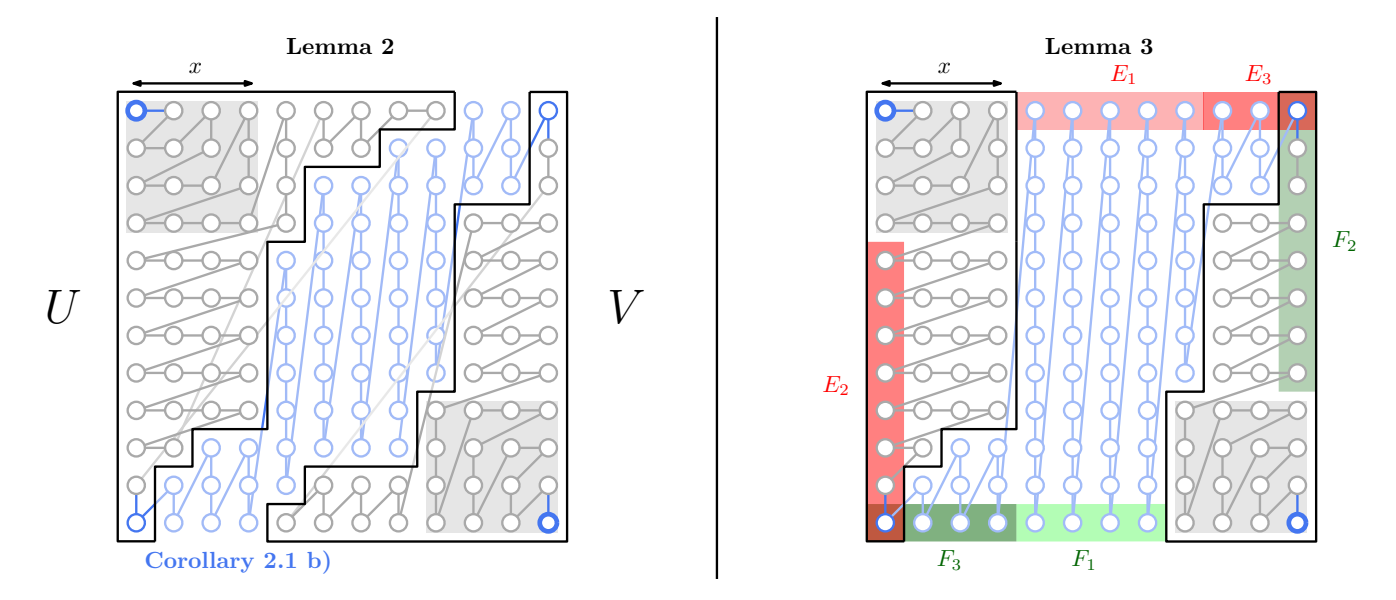


Figure 16: Lemma 3 shows how to delete regions of U and V so that the new enumeration scheme has a smaller edgesum C^1 .

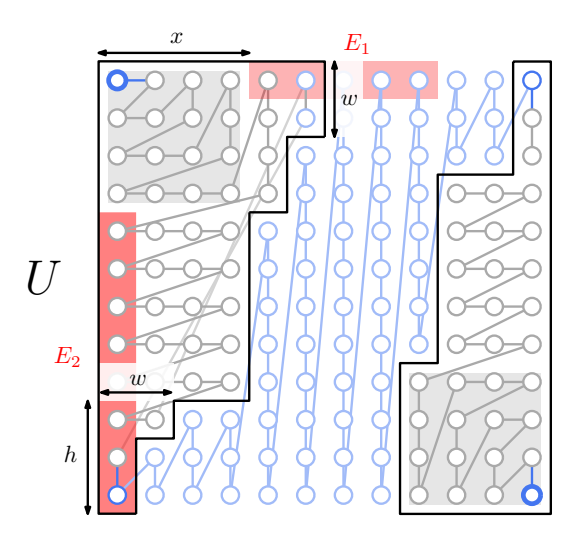


Figure 17: Deleting the rightmost column of U increases the value of $E_1 + E_2$.

Lemma 2. Suppose that the side lengths of the largest squares in U and V are both x. Then the edgesum of f is

$$C^{1}(f_{\rm M}) = N^{3} - xN^{2} + 2x^{2}N - \frac{2}{3}x^{3} + N^{2}$$

$$- xN - 2N + \frac{2}{3}x.$$
(40)

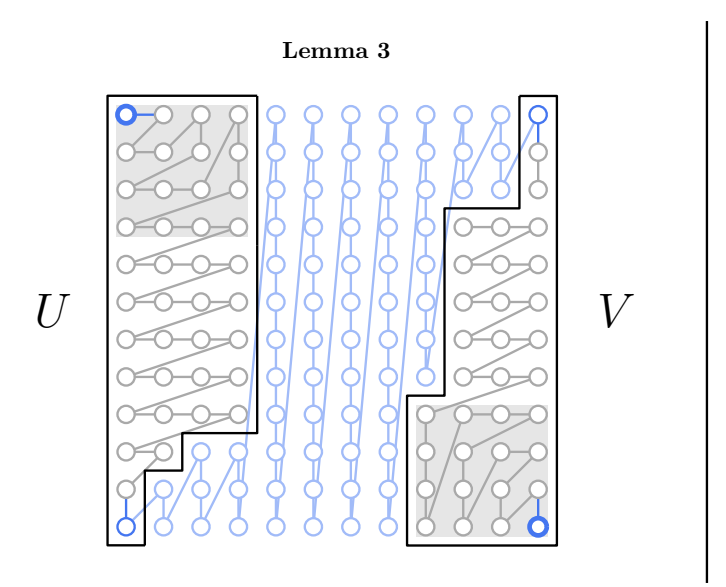
Proof. See Section III C 1.

Corollary 5.1. For $N \geq 5$, the value of x that minimises $C^1(f)$ in Equation 40 is $x = N - \frac{1}{2}\sqrt{2N^2 - 2N + \frac{4}{3}}$. Round x to the nearest integer to obtain the minimum $C^1(f)$ over all enumeration schemes for the $N \times N$ square lattice.

Proof. Treat N and x as continuous variables, and use calculus to find that minimum of $C^1(f)$ in Equation 40 occurs when $x = N - \frac{1}{2}\sqrt{2N^2 - 2N + \frac{4}{3}}$.

Note that the optimal value for x in Corollary 5.1 is a refinement on the value that Mitchison and Durbin give in [21]: they use the approximation $x = \left(1 - \frac{1}{\sqrt{2}}\right)N$. For all intents and purposes, these values are extremely close and rounding this approximate value for x gives the same integer as $N - \frac{1}{2}\sqrt{2N^2 - 2N + \frac{4}{3}}$ for most values of N.

Define the Mitchison-Durbin pattern $f_{\rm M}$ to be any of the optimal enumeration schemes that fill region U first



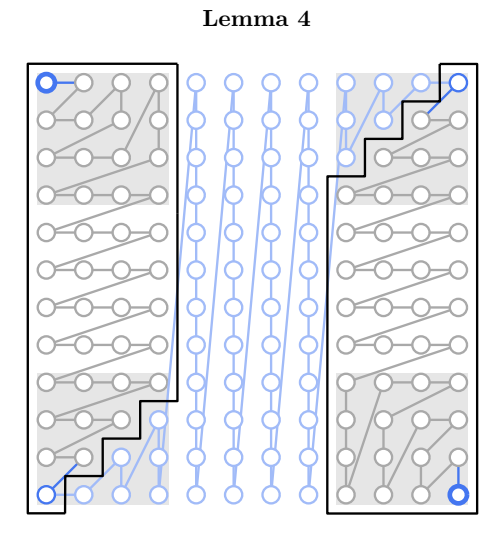


Figure 18: Lemma 4 shows the optimal shape for regions U and V in order to minimise the edgesum C^1 . The resulting pattern is the Mitchison-Durbin pattern $f_{\rm M}$.

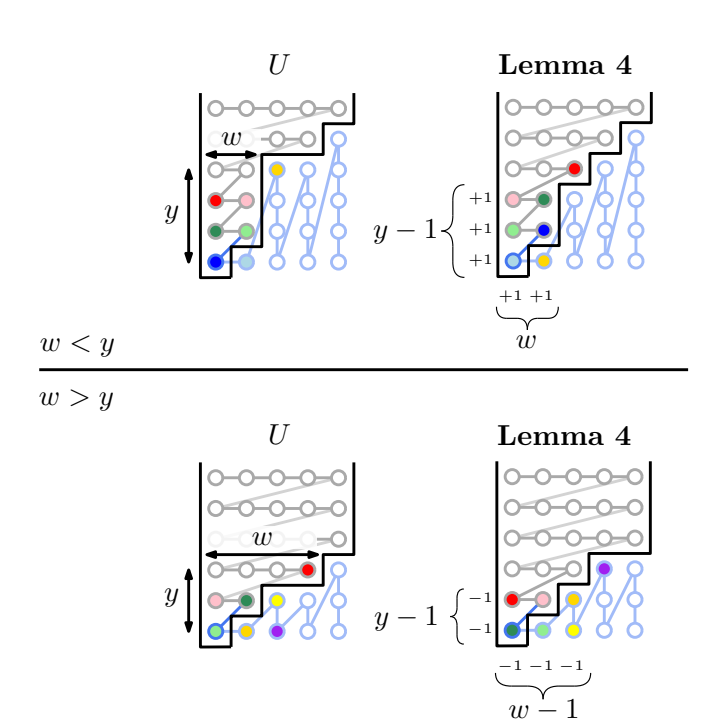


Figure 19: Modifying the shape of U in Lemma 4 to reduce the edge sum $\mathbb{C}^1.$

and region V last, where the value of N completely determines U and V via the successive restrictions of Lemmas 2–5 and Corollary 5.1. For example, in Figure 7, N=6 and x=2. In Figure 20, N=17 and x=5. This completes the proof.

1. Edgesum of the Mitchison-Durbin pattern

This section calculates the edge sum of the enumeration pattern f in Lemma 5. Divide the enumeration pattern on the $N \times N$ grid up into regions A, B, \ldots, G as in Figure 20. Let the label of each region also denote its edge sum. Therefore

$$C^{1}(f) = A + B + C + D + E + F + G$$

$$+ AB + AD + BD + BC + CD$$

$$+ DE + EF + DF + FG + DG,$$
(41)

where AB, \ldots, DG denote the sums of the differences between vertex labels across the interfaces between each pair of regions. Due to the symmetry of f, Equation 41 becomes

$$C^{1}(f) = 2(A + B + C) + D$$

$$+ 2(AB + AD + BC + BD + CD).$$
(42)

We can derive expressions for the contributions of each region to $C^1(f)$ by observing the patterns in the differences betwen vertex labels. Figure 21 shows the progression of vertex labels in regions A–D of the square lattice. Within each of these regions, the enumeration scheme is horizontally and vertically ordered. Thus, using Equation 35 on region A gives:

$$A = \left(\sum_{k=0}^{x-2} (x(x-2) + 2 + k) + \sum_{j=1}^{x} (x(x-1) + j)\right)$$
$$-\left(\sum_{k=1}^{x} (k(k-1) + 1) + \sum_{j=1}^{x} (j(j-2) + 2)\right) \quad (43)$$
$$= \frac{1}{6}(x-1)(6 + x(8x-1)). \quad (44)$$

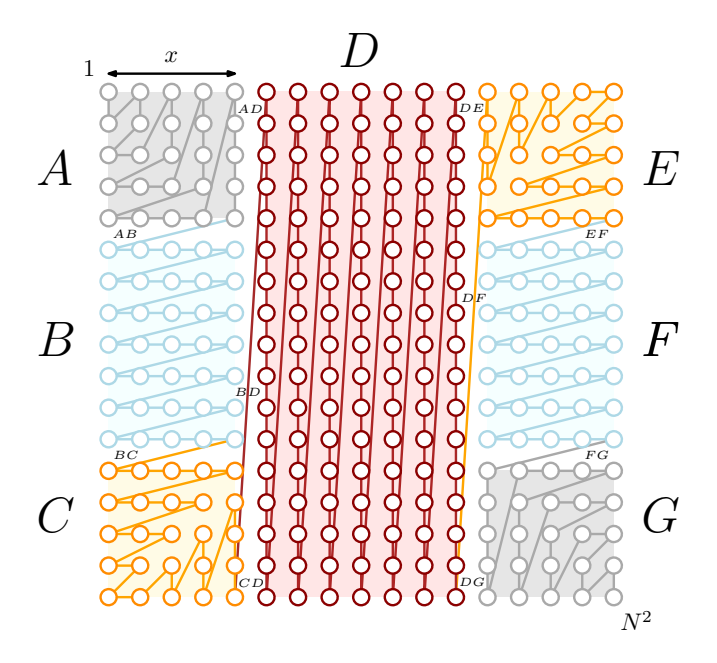


Figure 20: Sections of the $N \times N$ square lattice and an enumeration pattern f that satisfies Lemma 4.

The other regions contribute the following quantities:

$$B = (N - 2x)(x - 1) + x^{2}(N - 2x - 1)$$
 (45)

$$C = \frac{1}{6}(x-1)(6+x(8x-1)) \tag{46}$$

$$D = N^3 - 2xN^2 - 2xN + 2x - N. (47)$$

The vertex labels in Figure 21 also make it simple to calculate the contributions to $C^1(f)$ from the interfaces between the regions:

$$AD = \sum_{j=1}^{x} \left((x(x-1) + j) - (Nx + j) \right)$$
 (48)

$$= Nx^2 - x^3 + x^2 \tag{49}$$

$$AB = 1 - 2x + 2x^2 \tag{50}$$

$$BD = \frac{1}{2} \left(N^2 + N - 3xN + xN^2 + 2x^2 - 2x - 2x^2 N \right)$$

$$BC = x^2 (52)$$

$$CD = 1 - 2x + xN + x^2. (53)$$

Substituting Equations 44–53 into Equation 42 gives the result,

$$C^{1}(f_{\rm M}) = N^{3} - xN^{2} + 2x^{2}N - \frac{2}{3}x^{3} + N^{2}$$

$$-xN - 2N + \frac{2}{3}x.$$
(54)

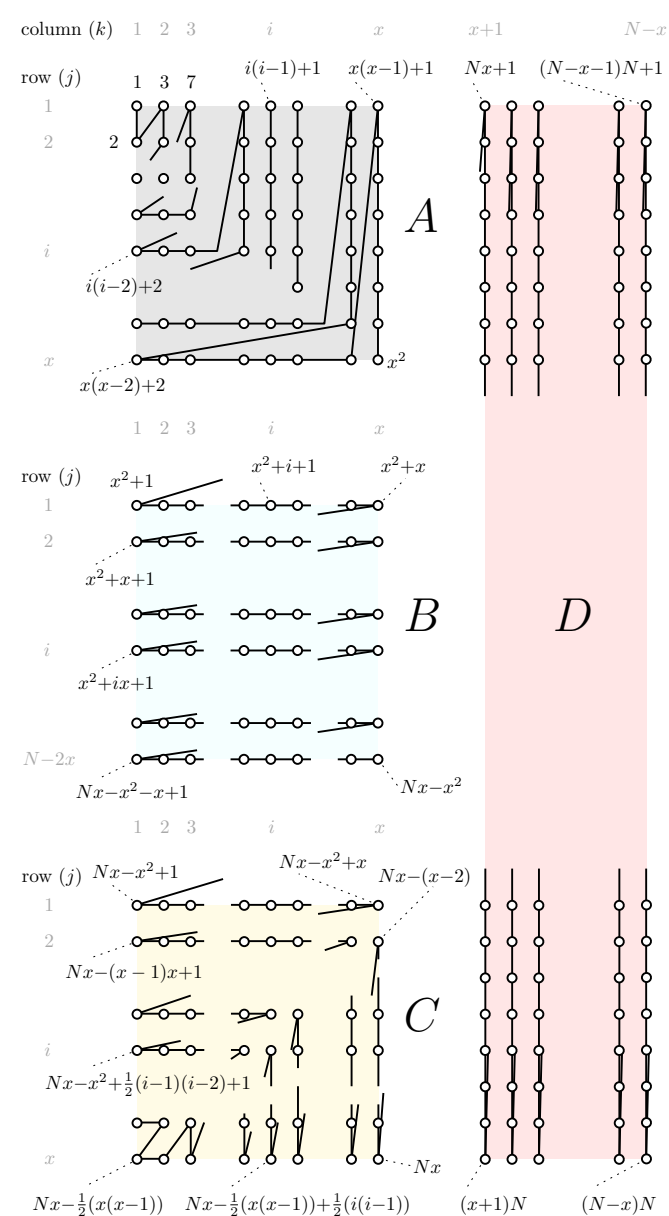


Figure 21: An in-depth look at the Mitchison-Durbin pattern $f_{\rm M}$. Vertex labels indicate the position of each vertex in the enumeration scheme.

D. Reducing the average Pauli weight for cellular fermion graphs

Theorem 1 reduces the average gate count of fermionic Hamiltonian simulation on a square lattice by making judicious use of the solutions to the edgesum problem. As Remark 2 discusses, there are only a handful of other graph families for which there are known edgesum solutions. It might be tempting to think that there is not much use in trying reduce average gate count via fermion enumeration scheme if the fermionic graph $G_{\rm F}$ does not belong to one of these families. In this section, however,

we show an example graph for which a "common-sense" approach to constructing a good enumeration scheme can provide an order-of-magnitude reduction in average gate count.

Consider $(n \times n) \times (N \times N)$ cellular arrangements of square fermionic lattices, where each $n \times n$ sub-lattice of fermions connects to adjacent sub-lattices via a single edge. Here we use the cellular pattern in Figure 22, where the connections are from each $n \times n$ lattice's top left vertex to the two closest vertices from neighbouring lattices.

It is possible to enumerate the fermions on a cellular arrangement graph with the Z-pattern $f_{\rm Z}$ or the S-pattern $f_{\rm S}$ from Section III B, treating the whole graph as a single square lattice. As Figure 22 shows, another way of enumerating the fermions is to number each sub-lattice before moving on to the next, progressing through the entire graph via an S- or Z-pattern. We call these two enumeration procedures $f_{\rm S'}$ and $f_{\rm Z'}$, respectively.

The edgesums of these enumeration schemes on the cellular arrangement graph are:

$$C^{1}(f_{S}) = \begin{cases} (Nn)^{3} - Nn - N(N-1)(n-1) - \sum_{k=0}^{N-1} \sum_{i=kn+2}^{(k+1)n} (2i-1), & n \text{ even} \\ (Nn)^{3} - Nn - N(N-1)(n-1) - \sum_{k=0}^{N-1} \sum_{i=kn+1}^{(k+1)n-1} (2i-1), & n \text{ odd,} \end{cases}$$
 (55)

$$C^{1}(f_{\mathbf{Z}}) = (Nn)^{3} - Nn - N(N-1)(n-1) - nN^{2}(n-1)(N-1),$$
(56)

$$C^{1}(f_{Z'}) = \begin{cases} N^{3}n^{2} + n^{3}N^{2} - n^{2}N^{2} - 2nN^{2} - n^{2}N + 2N^{2} + 2nN + n^{2} - 2N - n, & n \text{ even} \\ N^{3}n^{2} + n^{3}N^{2} - n^{2}N^{2} - nN^{2} - n^{2}N + N^{2} + 2nN + n^{2} - 2N - 2n + 1, & n \text{ odd,} \end{cases}$$
(57)

and while value of $C^1(f_{S'})$ also depends on the parities of n and N, it is strictly greater than $C^1(f_{Z'})$.

By using $f_{Z'}$ rather than f_Z , the edgesum of a large cellular arrengement graph reduces by an order of magnitude:

$$\lim_{N \to \infty} \frac{C^1(f_{Z'})}{C^1(f_Z)} = \frac{n^2}{n^3 - n^2 + n} = \mathcal{O}\left(\frac{1}{n}\right);$$
 (58)

$$\lim_{n \to \infty} \frac{C^1(f_{\mathbf{Z}'})}{C^1(f_{\mathbf{Z}})} = \frac{1}{N}.$$
 (59)

If $n = \mathcal{O}(N)$, then the graph has $\mathcal{O}(N^4)$ vertices. From choosing $f_{Z'}$ rather than f_Z , the $\mathcal{O}(1/N)$ factor reduction in edgesum is thus proportional to the fourth root of the number of vertices. This is a much more striking improvement than the constant-factor improvement that Corollary 1.1 proffers, even though we have not proved that $f_{Z'}$ is an optimal enumeration scheme for the cellular arrangement graph.

E. Reducing the average pth power of Pauli weight for a square lattice

In Section III A, we introduced other figures of merit for fermion enumeration schemes, such as the average pth power of Pauli weight for p > 1. For a given fermion graph $G_{\rm F}$, this corresponds to finding an enumeration scheme f that minimises the p-sum

$$C^{p}(f) = \left(\sum_{(u,v)\in E} |f(u) - f(v)|^{p}\right)^{1/p}.$$
 (60)

The p=1 case is the edge sum problem and via Remark 1 is NP–complete. George and Pothen showed that the minimum 2–sum problem is also NP–complete [30]. They develop spectral approaches to solving the minimum 1-sum and 2-sum problems for any graph $G_{\rm F}$. Separately, Mitchison and Durbin [21] explore the minimum p-sum problem where the graph $G_{\rm F}$ is a square lattice, and conclude with Proposition 2:

Proposition 2. (Mitchison and Durbin's results for the minimum p-sum problem on an $N \times N$ lattice [21]) Given a system of $n = N^2$ fermions interacting in a square $N \times N$ lattice G_F , the following are the lower limits for the value of $C^p(f)$:

- (a) If 0 , then there exists an enumeration scheme <math>f with $C^p(f) = \mathcal{O}(N^2)$.
- (b) If $\frac{1}{2} , then <math>C^p(f) \ge \frac{1}{2p+1}N^{1+2p} + \mathcal{O}(N^{2p})$.
- (c) If p=1, then f_M gives the minimum value as shown in Theorem 1.

(d) If
$$p > 1$$
, then $C^p(f) \ge \frac{4}{2^p(p+2)}N^{p+2}$.

The lower bounds in (b) and (d) are theoretical limits, and to date there are no known enumeration schemes that achieve their low coefficients. However, the "diagonal pattern" f_D has edgesum

$$C(f_{\rm D}) \approx \frac{4}{p+2} N^{p+2} + \mathcal{O}(N^{p+1}),$$
 (61)

which has the same order of magnitude in N as the theoretical limit in (d).

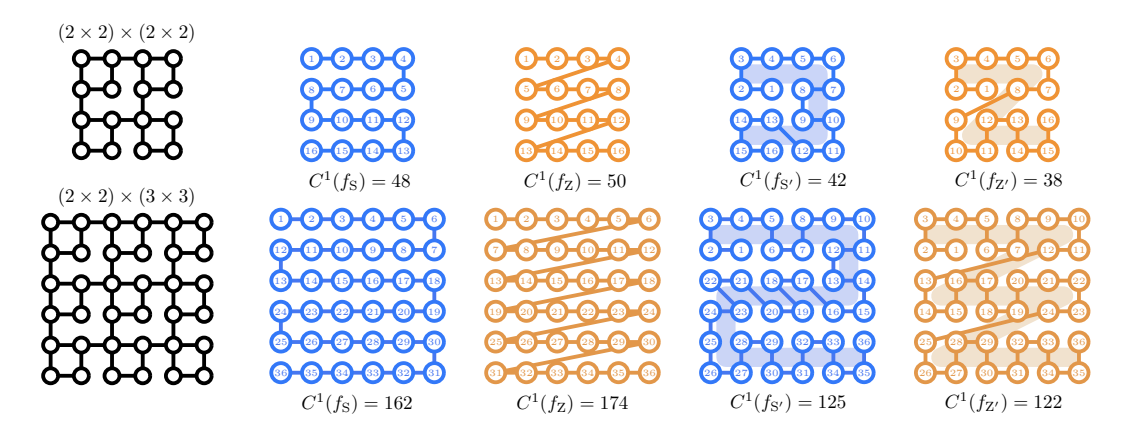


Figure 22: Edgesums for some enumeration schemes of $(n \times n) \times (N \times N)$ cellular arrangement patterns.

Enumeration scheme f	$C^1(f)$	$C^p(f), p > 1$
Mitchison-Durbin pattern $f_{\rm M}$	$N^{3} - xN^{2} + 2x^{2}N - 2x^{3}/3$ $+N^{2} - xN - 2N + 2x/3$	Includes terms $\geq \sim 2x^{p+1}N^p \sim 2k^{p+1}N^{2p+1}$ where $x = kN$
S-pattern $f_{\rm S}$	$N^3 - N$	$(N-1)\left(\sum_{k=1}^{N-1} (2k+1)^p + N + 1\right) \sim \frac{2^p}{p+1} N^{p+2} + \mathcal{O}(N^{p+1})$
Z-pattern $f_{\rm Z}$	$N^3 - N$	$(N-1)(N^{1+p}+N) = N^{p+2} - N^{p+1} + N^2 - N$
Diagonal pattern $f_{\rm D}$	$4N^3/3 - N^2 - N/3$	$2\left(\sum_{k=1}^{N-2} (2k+1)(k+1)^p + (N-1)N^p + 1\right) = \sim \frac{4}{p+2}N^{p+2} + \mathcal{O}(N^{p+1})$
		Theoretical limit $\sim \frac{4}{2^p(p+2)}N^{p+2} + \text{smaller}$

Figure 23: Results for the minimum p-sum problem for the square lattice for $p \ge 1$. While the Mitchison-Durbin pattern $f_{\rm M}$ minimises $C^p(f)$ for p = 1, it performs the worst of all the options for p > 1. The diagonal pattern $f_{\rm D}$ performs better than the rest for p > 2.

Proof. See Propositions 2–4 of [21].

Remark 3. (Best known results for the minimum p-sum problem on a square lattice, $p \ge 1$)

Figure 23 provides a table of known results for four enumeration schemes $f_{\rm S}$, $f_{\rm M}$, $f_{\rm Z}$, and $f_{\rm D}$ (the diagonal pattern) in the regimes p=1 and p>1. The diagonal pattern is the solution to the bandwidth problem (from Section II E) on rectangles [21], and is the best-performing pattern for the minimum p-sum problem for p>1, $N\to\infty$.

IV. IMPROVING BEYOND OPTIMALITY WITH ANCILLA QUBITS

All of the techniques in Section III have permitted only as many qubits as there are fermions. Theorem 1, for example, details the optimal Jordan-Wigner mapping for the task if one is restricted to using N^2 qubits to simulate an $N \times N$ fermionic lattice. However, permitting

m>n qubits, there is a competitive interplay between the qubit- and gate-count resource costs of fermion-qubit mappings. As qubits are highly costly with current technology, the qubit-gate tradeoff begs the question: how many gates is it possible to eliminate by using an extra qubit?

Moll et al. [35] show how to reduce the number of qubits in a Jordan-Wigner mapping at the cost of introducing more terms into the molecular Hamiltonian, thus increasing quantum gate count. Auxiliary qubit mappings [12, 15, 16, 19, 36] show the converse: that by introducing more qubits into a simulation it is possible to vastly simplify the Hamiltonian. Verstraete and Cirac showed that a system combining an $N \times N$ 2D qubit lattice with N^2 ancilla qubits can, using local qubit operations, simulate a fermionic lattice Hamiltonian [12]. That is, rather than producing long strings of Pauli terms of weight $\mathcal{O}(N)$ that wind around the qubit lattice (as in, for example, Figure 29), the auxiliary qubit mappings produce operations of weight $\mathcal{O}(1)$ and act on adjacent

qubits. This comes at the cost of using twice as many qubits as in the original simulation.

In Section IV A, we describe Steudtner and Wehner's template for auxiliary qubit mappings [16]. In Section IV B, we give an example of this process in the form of a new auxiliary qubit mapping. We augment the Mitchison-Durbin pattern to achieve a 40% reduction over the S-pattern's average Pauli weight, using only two extra qubits. Thus, taking advantage of Mitchison-Durbin mapping we see that a constant number of additional qubits almost triples the advantage provided by Theorem 1.

A. Auxiliary qubit mappings

Steudtner and Wehner's formulation of auxiliary qubit mappings [16] is thus: suppose H is a Hamiltonian

$$H = \sum_{h \in \Gamma} \alpha_h h \,, \tag{62}$$

where $\Gamma \subset \{1, X, Y, Z\}^{\otimes n}$ and $\alpha_h \in \mathbb{C}$ so that H is Hermitian, is acting on an n-qubit data system (which we denote by the subscript 'dat'). Given a state $|\psi\rangle_{\mathrm{dat}}$ of the qubit system, the goal is to simulate time evolution $e^{-iHt}|\psi\rangle_{\mathrm{dat}}$ using as few quantum gates as possible. An auxiliary qubit mapping is a carefully-constructed fermion-qubit mapping which achieves this goal using ancilla qubits in an auxiliary register (which we denote by the subscript 'aux'). The following three steps detail how to construct a straightforward type of auxiliary qubit mapping along with the requirements in order for it to function.

1. Choose a subset $\Gamma_{\text{non-loc}} \subset \Gamma$ of terms in the Hamiltonian H. These are the terms which the auxiliary qubit mapping will shorten. For each $h \in \Gamma_{\text{non-loc}}$, choose a Pauli string p^h where $h = h_{\text{loc}} p^h$ such that the weight of h_{loc} is less than that of h. In total, only use r distinct p-strings. That is, several $h \in \Gamma_{\text{non-loc}}$ may contain the same p^h .

Denote the set of all p^h by $\{p_i\}_{i=1}^r$. That is, for any $h \in \Gamma_{\text{non-loc}}$, then $p^h = p_i$ for some $i \in \{1, \dots, r\}$.

2. Introduce r ancilla qubits in the auxiliary register, and devise a unitary mapping

$$V: |\psi\rangle_{\mathrm{dat}} |0\rangle_{\mathrm{aux}}^{\otimes r} \mapsto |\widetilde{\psi}\rangle_{\mathrm{dat,aux}}$$
 (63)

where $|\widetilde{\psi}\rangle_{\mathrm{dat,aux}}$ is such that for each $i\in\{1,\ldots,r\}$, there exists $\sigma_i\in\{1,X,Y,Z\}$ acting on the ith auxiliary qubit such that

$$((p_i)_{\text{dat}} \otimes (\sigma_i)_{\text{aux}})|\widetilde{\psi}\rangle_{\text{dat,aux}} = |\widetilde{\psi}\rangle_{\text{dat,aux}}.$$
 (64)

The $p_i \otimes \sigma_i$ are the *stabilisers* of the combined data and auxiliary system.

Requirement 1: The choice of $\{p_i\}_{i=1}^r$ must allow for the existence of $|\widetilde{\psi}\rangle_{\text{dat,aux}}$ obeying Equation 64. A necessary but insufficient condition is that $[p_i, p_j] = 0$ for all $i, j \in \{1, \dots, r\}$.

3. Modify each $h \in \Gamma$ via

$$h_{\rm dat} \longmapsto h_{\rm dat} \otimes \kappa_{\rm aux}^h \,, \tag{65}$$

where κ^h is a Pauli string acting on the auxiliary qubits such that

$$[h_{\rm dat} \otimes (\kappa^h)_{\rm aux}, (p_i)_{\rm dat} \otimes (\sigma_i)_{\rm aux}] = 0$$
 (66)

for all $i \in \{1, ..., r\}$. The rationale for this step is as follows: Suppose that $h = h_{\text{loc}} p^h$, where $p^h = p_i$. Then, we can multiply each $h = h_{\text{loc}} p^h \in \Gamma_{\text{non-loc}}$ by its corresponding stabiliser, thus producing a lower-weight Hamiltonian term, $((h_{\text{loc}})_{\text{dat}} \otimes (\sigma_i)_{\text{aux}})$:

$$(h_{\rm dat} \otimes \mathbb{1}_{\rm aux}) |\widetilde{\psi}\rangle_{\rm dat,aux}$$
 (67)

 $= \left((h_{\mathrm{loc}} \, p^h)_{\mathrm{dat}} \otimes \mathbb{1}_{\mathrm{aux}} \right) |\widetilde{\psi}\rangle_{\mathrm{dat,aux}}$

$$= ((h_{\text{loc}} p_i)_{\text{dat}} \otimes \mathbb{1}_{\text{aux}}) |\widetilde{\psi}\rangle_{\text{dat,aux}}$$
 (68)

$$= ((h_{\rm loc} p_i)_{\rm dat} \otimes \mathbb{1}_{\rm aux}) \tag{69}$$

$$((p_i)_{\mathrm{dat}} \otimes (\sigma_i)_{\mathrm{aux}}) |\widetilde{\psi}\rangle_{\mathrm{dat,aux}}$$

$$= ((h_{\rm loc})_{\rm dat} \otimes (\sigma_i)_{\rm aux}) |\widetilde{\psi}\rangle_{\rm dat, aux}.$$
 (70)

To replicate the time evolution $e^{-iHt}|\psi\rangle_{\rm dat}$ of the system, it is necessary to be able to generate any stabiliser $((p_j)_{\rm dat}\otimes(\sigma_j)_{\rm aux})$ at the step in Equation 69 and commute it past any Hamiltonian term $h_{\rm dat}\otimes\mathbb{1}_{\rm aux}$ where h can now be any element of Γ . If $[h_{\rm dat}\otimes\mathbb{1}_{\rm aux},(p_j)_{\rm dat}\otimes(\sigma_j)_{\rm aux}]=[h,p_j]\neq 0$, then application of the Hamiltonian term produces a state

$$|\widetilde{\psi}'\rangle_{\text{dat aux}} = (h_{\text{dat}} \otimes \mathbb{1}_{\text{aux}}) |\widetilde{\psi}\rangle_{\text{dat,aux}}$$
 (71)

that no longer satisfies Equation 64 for all i, and thus it is impossible to generate and apply more stabilisers as required by Equation 69.

Requirement 2: Crucially, the κ^h must be such that they preserve the time evolution of the data system. That is,

$$V^{\dagger}(h_{\text{dat}} \otimes (\kappa^{h})_{\text{aux}}) |\widetilde{\psi}\rangle_{\text{dat,aux}}$$

$$= h |\psi\rangle_{\text{dat}} \otimes |0\rangle_{\text{aux}}^{\otimes r} .$$
(72)

Otherwise, the system would not retain any useful information. The requirement for the existence of κ^h for $h \in \Gamma$ places a restriction on V.

After satisfying the above three steps, observe that

$$(e^{-iHt} |\psi\rangle_{\rm dat}) \otimes |0\rangle_{\rm aux}^{\otimes r} = (V^{\dagger} e^{-i\widetilde{H}t}) |\widetilde{\psi}\rangle_{\rm dat,aux} , \quad (73)$$

 $^{^1}$ Other classes of auxiliary qubit mappings exist. For example, the Verstraete-Cirac mapping uses stabilisers that are of the form $p_{\rm dat} \otimes \tau_{\rm aux}$ where $\tau_{\rm aux}$ acts on more than one qubit [12].

where the effective qubit Hamiltonian \hat{H} achieves the goal of reducing the Pauli weight of the strings in $\Gamma_{\text{non-loc}}$, and acts on both the data and auxiliary systems:

$$\widetilde{H} = \sum_{h \in \Gamma_{\text{non-loc}}} \alpha_h \left((h_{\text{loc}})_{\text{dat}} \otimes (\kappa^h \sigma^h)_{\text{aux}} \right)$$

$$+ \sum_{h \in \Gamma \setminus \Gamma_{\text{non-loc}}} \alpha_h (h_{\text{dat}} \otimes (\kappa^h)_{\text{aux}}).$$
(74)

In Equation 74, the Pauli gate σ^h is the gate σ_i from the stabiliser $p_i \otimes \sigma_i$ corresponding to $h = h_{\rm loc} \, p^h$ via $p^h = p_i$. Assuming the cost of implementing V is insignificant compared to cost of implementing time evolution by \widetilde{H} , then Equation 73 shows the advantage of the auxiliary qubit mapping: $V^{\dagger}e^{-i\widetilde{H}t}$ is less costly to implement than e^{-iHt} .

B. Using 2 ancilla qubits to reduce average Pauli weight by 40% compared to S-pattern

By modifying the proposal in Theorem 1, it is possible to use the Mitchison-Durbin pattern to produce a 'super-efficient' mapping for square fermionic lattices that is significantly more local, using just $N^2 + 2$ qubits. The result presented here has an average Pauli weight approximately 30% less than our result in Theorem 1, and approximately 40% less than that of the original Spattern in [12].

Begin by observing that the edgesum $C^1(f_{\rm M})$ of the Mitchison-Durbin pattern has two costly contributions: the $\mathcal{O}(x^2N)$ -valued difference between adjacent vertices in the AD- and DG-interfaces as labelled in Figure 20. We will construct an auxiliary qubit mapping to reduce the contributions of these edges to $C^1(f_{\rm M})$.

Take the Hamiltonian of the $N \times N$ square fermionic lattice,

$$H_{\text{fermion}} = \sum_{(\alpha,\beta) \in E} a_{\alpha}^{\dagger} a_{\beta} , \qquad (75)$$

where $G_{\rm F}=(V,E)$ is the $N\times N$ square lattice. Next, Jordan-Wigner transform $H_{\rm fermion}$ into a qubit Hamiltonian acting on the data register,

$$H = \sum_{h \in \Gamma} h \,, \tag{76}$$

where Γ is the set of Pauli strings produced by the Mitchison-Durbin pattern's enumeration of the vertices of $G_{\rm F}$, as in Figure 7. However, with $C^1(f_{\rm M})$ being the expression in Equation 26, do not use the previous optimal value for $x \ (\approx 0.29N)$ from Corollary 5.1 and instead treat $x \in \{1, 2, \ldots, N\}$ as a variable which is yet to be determined.

Our fermion-qubit mapping uses a similar approach to the E-type auxiliary qubit mapping from [16]. We will follow the formulation of auxiliary qubit mappings in Section IV:

1. Choose p-strings $\{p_1, p_2\}$ that correspond to the longest individual strings of Z-gates of any term $h \in \Gamma$. In this case, we choose

$$p_1 = \left(\bigotimes_{i=x(x-1)+2}^{xN} Z_i\right) \otimes \left(\bigotimes_{\text{other}} \mathbb{1}_i\right) \tag{77}$$

$$p_2 = \left(\bigotimes_{i=(N-x)N+1}^{N^2-x^2+x-1} Z_i\right) \otimes \left(\bigotimes_{\text{other } i} \mathbb{1}_i\right). \tag{78}$$

These bridge the gaps between the outermost vertices on the AD- and DG-interfaces, respectively. Figure 24 depicts the two p-strings; the indices of the first and last qubits of each p-string result from inspecting the label guide in Figure 21.

Then, define $\Gamma_{\text{non-loc}}$ to be all the Hamiltonian terms $h \in \Gamma$ that contain less Z gates upon multiplication by either p_1 or p_2 . Note that none of the $h \in \Gamma$ would benefit from multiplication by both p-strings. These p-strings trivially satisfy **Requirement 1**'s preliminary condition that $[p_1, p_2] = 0$.

2. Introduce two auxiliary qubits, labelled $N^2 + 1$ and $N^2 + 2$. Define the unitary mapping V to be a cascade of controlled-NOT operations, storing the net parity of the qubits appearing in p_i in the phase of the ith auxiliary qubit. Figure 25 shows a valid circuit for V.

For any input state $|\psi\rangle_{\rm dat}$ of the original $N^2{\rm -qubit}$ system, now consider the state

$$|\widetilde{\psi}\rangle_{\text{dat.aux}} = V |\psi\rangle_{\text{dat}} |0\rangle_{\text{aux}}^{\otimes 2} .$$
 (79)

This state has two stabilisers:

$$((p_1)_{\mathrm{dat}} \otimes (Z \otimes 1)_{\mathrm{aux}}) |\widetilde{\psi}\rangle_{\mathrm{dat,aux}} = |\widetilde{\psi}\rangle_{\mathrm{dat,aux}}, \quad (80)$$

$$((p_2)_{\rm dat} \otimes (\mathbb{1} \otimes Z)_{\rm aux}) |\widetilde{\psi}\rangle_{\rm dat, aux} = |\widetilde{\psi}\rangle_{\rm dat, aux} . \tag{81}$$

The existence of the stabiliser state $|\widetilde{\psi}\rangle_{\rm dat,aux}$ satisfies Requirement 1.

3. To identify which terms $h \in \Gamma$ do not commute with p_1 and p_2 , recall from Equation 16 that, without loss of generality, hopping terms have the form

$$h_{\mathrm{dat}} = (X \otimes Z \otimes \cdots \otimes Z \otimes X) \otimes \left(\bigotimes_{\mathrm{other}} \mathbb{1}\right).$$
 (82)

As p_1 and p_2 comprise only Z gates, $[h, p_i] = 0$ if and only if the Pauli string XZZ...ZX of h intersects completely, or not at all, with the Pauli string ZZZ...Z of p_i , because $[X,Z] = -2Y \neq 0$. Thus the vast majority of the hopping terms already commute with both p-strings; it is only the hopping terms that have one end 'in' p_i and one end 'out of' p_i that need to change. If $[h, p_1] \neq 0$, make the adjustment

$$h_{\mathrm{dat}} \longmapsto h_{\mathrm{dat}} \otimes (X \otimes \mathbb{1})_{\mathrm{aux}} ;$$
 (83)

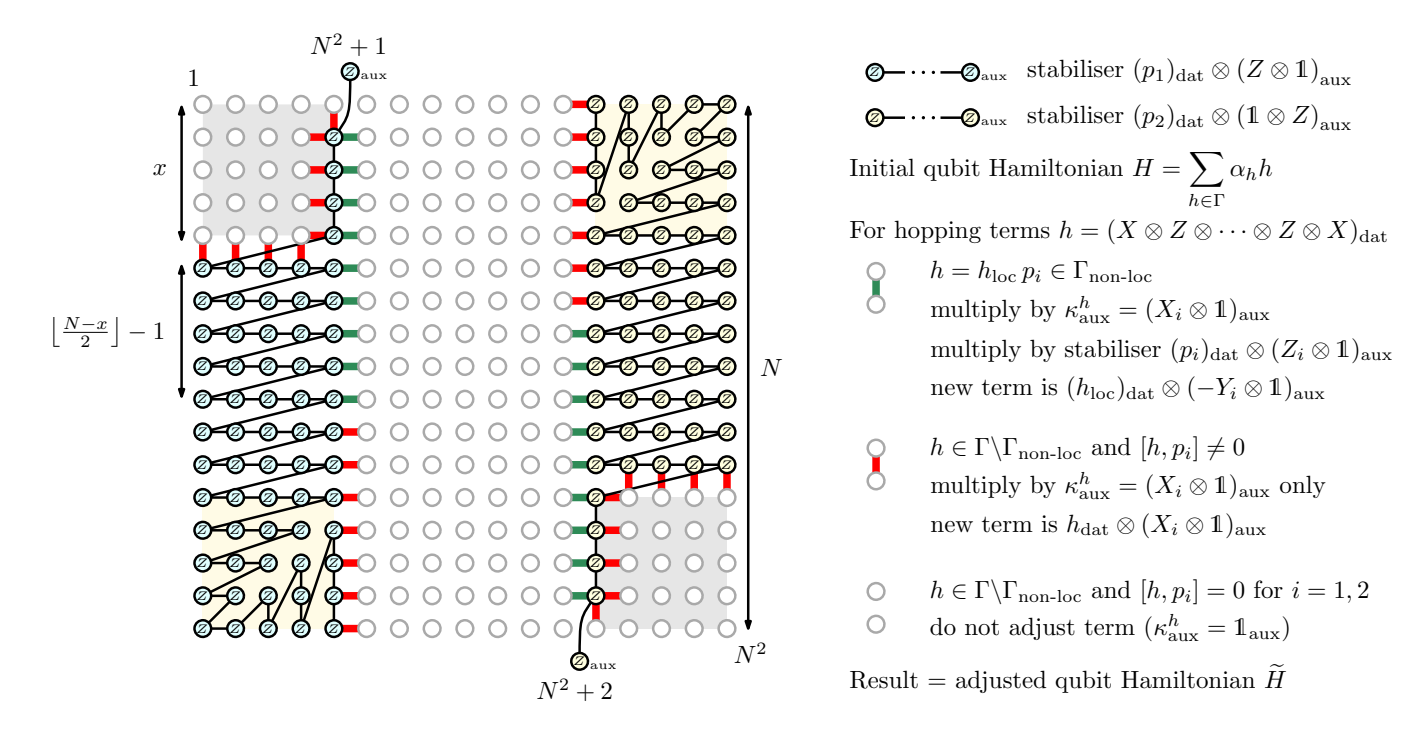


Figure 24: Stabilisers and adjusted Hamiltonian hopping terms for the auxiliary qubit mapping using our augmented Mitchison-Durbin pattern, ' f_{M+2} '. Initialising the (N^2+2) -qubit system in a state stabilised by the strings $p_i \otimes \sigma_i$ nullifies the most costly contributions to the edgesum of the Mitchison-Durbin pattern, resulting in a significantly more local Hamiltonian \widetilde{H} .

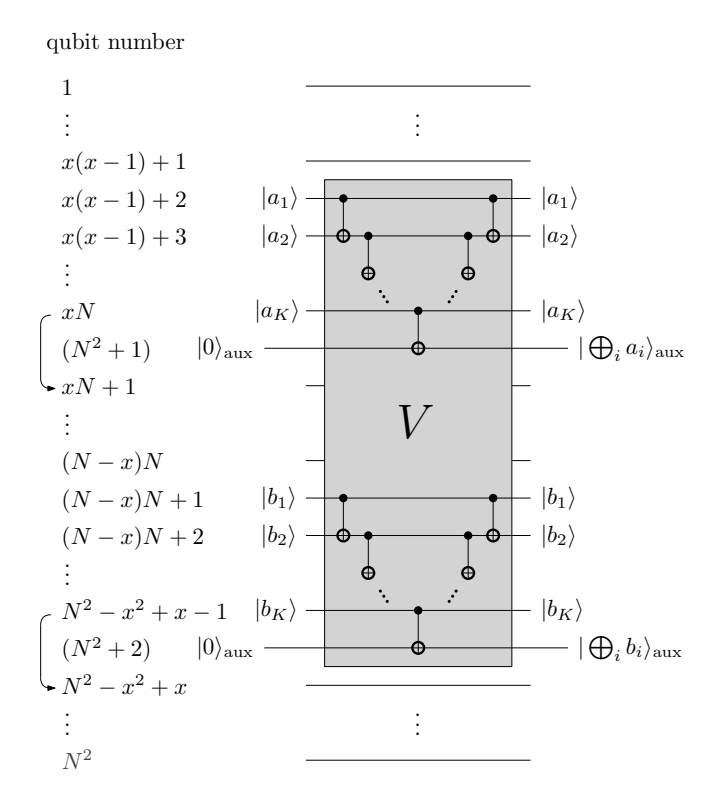


Figure 25: A circuit for V, which initialises the stabiliser state $|\widetilde{\psi}\rangle_{\rm dat,aux}$ from $|\psi\rangle_{\rm dat}|0\rangle_{\rm aux}^{\otimes 2}$ while preserving the time-evolution of the underlying data system.

if $[h, p_2] \neq 0$, make the adjustment

$$h_{\mathrm{dat}} \longmapsto h_{\mathrm{dat}} \otimes (\mathbb{1} \otimes X)_{\mathrm{aux}} .$$
 (84)

Note that no more than one of these corrections need be made to any hopping term h on the lattice, due to the spatial separation of p_1 and p_2 . Abbreviating the correction by κ^h , each adjusted Hamiltonian term then satisfies

$$[h_{\text{dat}} \otimes \kappa_{\text{aux}}^h, (p_i)_{\text{dat}} \otimes (\sigma_i)_{\text{aux}}] = 0$$
 (85)

for i = 1, 2 because $[X_{\text{dat}} \otimes X_{\text{aux}}, Z_{\text{dat}} \otimes Z_{\text{aux}}] = 0$. Figure 24 shows which hopping terms need adjustment in this way.

Finally, check that V and κ^h satisfy **Requirement** 2. Let h be a hopping term that does not commute with p_1 . Consider an arbitrary input state

$$|\psi\rangle_{\text{dat}} = \sum_{\vec{q}\ \vec{b}} \gamma |a_1 a_2 \dots, b_1 b_2 \dots, c_1 c_2 \dots\rangle_{\text{dat}} , \quad (86)$$

where $a_j, b_j, c_j \in \{0, 1\}$ such that \vec{a} contains the parities of all the qubits involved in p_1, \vec{b} contains the parities of the qubits not involved in either p-string, and \vec{c} contains the parities of the qubits involved in p_2 . The coefficient $\gamma \in \mathbb{C}$ depends on the bit strings \vec{a}, \vec{b} and \vec{c} .

As h does not commute with p_1 , it must perform an X gate on one qubit from \vec{a} and one from from \vec{b} .

Let these be the jth and kth qubits in each string, respectively. Therefore, the output of $h |\psi\rangle_{\text{dat}}$ is

$$h |\psi\rangle_{\text{dat}} = \sum_{\vec{a},\vec{b}} \gamma' |a_1...\overline{a_j}..., b_1...\overline{b_k}..., c_1c_2...\rangle_{\text{dat}}, \quad (87)$$

where γ' is equal to γ up to a sign depending on the effect of the Z gates in h. Meanwhile, our prescription for κ^h is to apply an X on the first auxiliary qubit. Noting that $V = V^{\dagger}$, observe that

$$V(h \otimes \kappa^h) |\widetilde{\psi}\rangle = V(h \otimes \kappa^h) \sum_{\vec{a} \ \vec{b}} \gamma |a_1 a_2 \dots, b_1 b_2 \dots, c_1 c_2 \dots\rangle_{\text{dat}} \otimes (|\oplus_l a_l\rangle |\oplus_l c_l\rangle)_{\text{aux}}$$
(88)

$$= V \sum_{\vec{a}, \vec{b}} \gamma' \left| a_1 \dots \overline{a_j} \dots, b_1 \dots \overline{b_k} \dots, c_1 c_2 \dots \right\rangle_{\text{dat}} \otimes \left(\left| \overline{\bigoplus_l a_l} \right\rangle \left| \bigoplus_l c_l \right\rangle \right)_{\text{aux}}$$
(89)

$$= V \sum_{\overline{a}, \overline{b}} \gamma' \left| a_1 \dots \overline{a_j} \dots, b_1 \dots \overline{b_k} \dots, c_1 c_2 \dots \right\rangle_{\text{dat}} \otimes \left(\left| a_1 \oplus \dots \oplus \overline{a_j} \oplus \dots \right\rangle \left| \oplus_l c_l \right\rangle \right)_{\text{aux}}$$
(90)

$$= \sum_{\vec{a}, \vec{b}} \gamma' \left| a_1 \dots \overline{a_j} \dots, b_1 \dots \overline{b_k} \dots, c_1 c_2 \dots \right\rangle_{\text{dat}} \otimes (|0\rangle |0\rangle)_{\text{aux}}$$

$$(91)$$

$$= h |\psi\rangle_{\text{dat}} \otimes |0\rangle_{\text{aux}}^{\otimes 2} \tag{92}$$

as required. Progressing from Equation 90 to Equation 91 uses fact that V is a cascade of controlled-NOT gates. A symmetric argument follows for all $h \in \Gamma$ which do not commute for p_2 .

This establishes a valid auxiliary qubit mapping. In order to compare the results of this scheme to the ancilla-free approach in Theorem 1, and to the original S-pattern proposal in [12], let us compute the modified Hamiltonian's average Pauli weight.

The total Pauli weight of all terms in the modified Hamiltonian \widetilde{H} is (1) the cost of the original H, plus (2) the difference between the new and old Z-gate counts of the terms in $\Gamma_{\text{non-loc}}$ after multiplication by stabilisers, plus (3) the cost of extra gates on the auxiliary qubits from making the κ^h adjustments to terms in $\Gamma \backslash \Gamma_{\text{non-loc}}$. That is,

Total Pauli weight of \tilde{H} (93)

- = (1) Total Pauli weight of H
 - + (2) difference in Z gate count of \widetilde{H} and H
 - + (3) number of adjusted terms in \widetilde{H} that are not multiplied by stabilisers

Begin by only considering the effects of the first stabiliser, $(p_1)_{\rm dat} \otimes (Z \otimes 1)_{\rm aux}$.

For (1), recall from Equation 23 that the total Pauli weight of the square lattice qubit Hamiltonian H is $C^1(f_{\rm M}) + 2N(N-1)$.

For (2): we explain which hopping terms should be multiplied by stabilisers here. In the original Hamiltonian H, a term $h \in \Gamma$ between vertices α and β of G_F has Pauli weight $|f_{\rm M}(\alpha) - f_{\rm M}(\beta)| + 1$; as hopping terms

consist of a string of Z gates between single X or Y gates, the total number of Z gates in such a term is then

$$\#(Z \text{ gates in } h) = |f_{\mathcal{M}}(\alpha) - f_{\mathcal{M}}(\beta)| - 1.$$
 (94)

Referring to the region labels A,B,...,D in Figure 21, it is clear that all of the lengthy hopping terms between vertices on the AD-interface will have less Z gates after multiplication by the stabiliser $(p_1)_{\rm dat}\otimes (Z\otimes 1)_{\rm aux}$. Using the labels from Figure 21 in Equation 94, the original number of Z gates in each of these terms is then

$$\#(Z \text{ gates in } AD, before) = Nx - x(x-1) - 1.$$
 (95)

By inspection, the topmost hopping term across the AD-interface after multiplication by $(p_1)_{\text{dat}} \otimes (Z \otimes \mathbb{1})_{\text{aux}}$ will consist of a single Z gate on the first auxiliary qubit. For the hopping terms across the AD-interface in the ith row beneath the top row, there will be 2i Z gates after multiplication by $(p_1)_{\text{dat}} \otimes (Z \otimes \mathbb{1})_{\text{aux}}$, including the gate on the auxiliary qubit.

For the hopping term across the ith row in the BD–interface, once again using labels from Figure 21 in Equation 94 yields

$$\#(Z \text{ gates in BD}, before) = Nx + x + i - (x^2 + ix + 1).$$
(96)

By inspection, these terms will have (2+i)x+i-2 Z-gates after multiplication by the stabiliser $(p_1)_{\rm dat}\otimes(Z\otimes 1)_{\rm aux}$, including the gate on the auxiliary qubit. Then, we reduce the Z-gate count count of the BD-interface hopping terms as long as

$$(2+i)x+i-2 < Nx+x+i-(x^2+ix+1)$$
 (97)

$$i < \frac{N - x - 1}{2} \,. \tag{98}$$

Average Pauli weights of enumeration schemes $(N \times N \text{ lattice})$

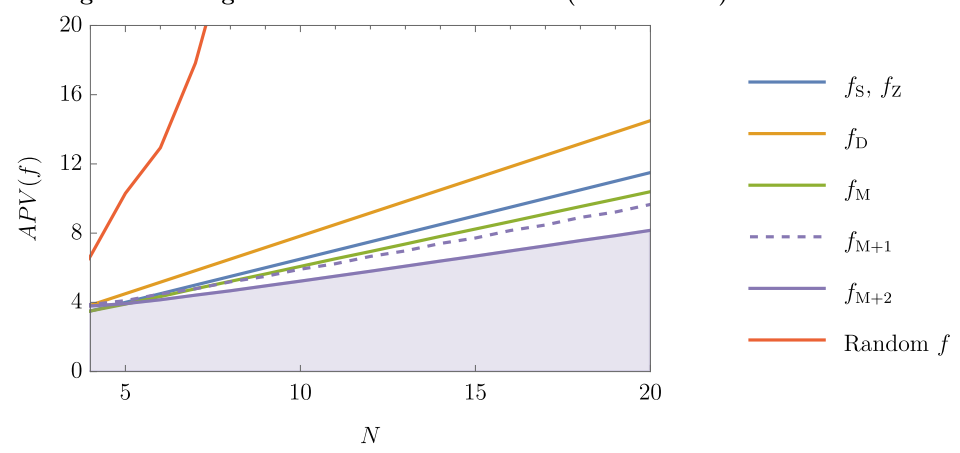


Figure 26: Average Pauli weights APV(f) of enumeration schemes on $N \times N$ lattices. The auxiliary qubit patterns f_{M+1} and $f_{\rm M+2}$ outperform the ancilla-free optimal enumeration pattern $f_{\rm M}$ using only a 1 or 2 extra qubits, respectively.

For this reason, only the hopping terms across the first (|(N-x)/2|-1) rows of the BD-interface need to be multiplied by stabilisers, as Figure 24 shows.

For (3), note that we must adjust all of the hopping terms h that do not commute with p_1 by multiplication by κ^h , a single X gate in first auxiliary qubit. However, in (2) we have already accounted for the cost of an extra auxiliary Z gate on each of the terms in the AD- and BD-interfaces that benefitted from stabiliser multiplication. This Z gate will become (-Y)upon prior adjustment κ^h (multiplication by X). We

therefore only need to count any remaining hopping terms that only partially overlap with p_1 : by inspection of Figure 24, the total number of such terms is 2x-1+(N-x-(|(N-x)/2|-1)=N+x-|(N-x)/2|.

As the Mitchison-Durbin pattern is symmetric, the same rules apply when considering the effects of the second stabiliser, $(p_2)_{\rm dat} \otimes (\mathbb{1} \otimes Z)_{\rm aux}$. We can now finally substitute these values into Equation 93 and express the total Pauli weight of H. Note that the factor of 2 in Equation 99 takes into account both stabilisers:

Total Pauli weight of \widetilde{H}

Total Pauli weight of
$$H$$
 (99)

$$= C^{1}(f_{M}) + 2N(N-1) + 2\left(\left(1 - (Nx - x(x-1) - 1) + \sum_{i=1}^{x-1} (2i - (Nx - x(x-1) - 1)) + \sum_{i=1}^{x-1} ((2i - (Nx - x(x-1) - 1)) + \sum_{i=1}^{x-1} ((2i - (Nx - x(x-1) - 1))) + \sum_{i=1}^{x-1} ((2i - (Nx - x(x-1) - 1)) + \sum_{i=1}^{x-1} ((2i - (Nx - x(x-1) - 1)) + \sum_{i=1}^{x-1} ((2i - (Nx - x(x-1) - 1)) + \sum_{i=1}^{x-1} ((2i - (Nx - x(x-1) - 1)) + \sum_{i=1}^{x-1} ((2i - (Nx - x(x-1) - 1)) + \sum_{i=1}^{x-1} ((2i - (Nx - x(x-1) - 1)) + \sum_{i=1}^{x-1} ((2i - (Nx - x(x$$

An approximately optimal value of x to minimise Equation 100 is

$$x = \frac{1}{5} \left(4 - 2N + \frac{\sqrt{57N^2 - 78N - 32}}{\sqrt{3}} \right)$$
 (101)

$$\approx 0.47N,$$
 (102)

which is the result of removing the floor brackets. This is significantly greater than the optimal value of $x \approx 0.29N$ from Corollary 5.1, where there were no auxiliary qubits

Comparing our auxiliary qubit mapping, here nicknamed ' f_{M+2} ', to the S-pattern of [12] and the Mitchison-Durbin pattern of Theorem 1,

$$\lim_{N \to \infty} \frac{APV(f_{\rm M+2})}{APV(f_{\rm S})} \approx 0.60 \tag{103}$$

$$\lim_{N \to \infty} \frac{APV(f_{\text{M}+2})}{APV(f_{\text{M}})} \approx 0.70, \qquad (104)$$

yielding a 40% improvement over the S-pattern.

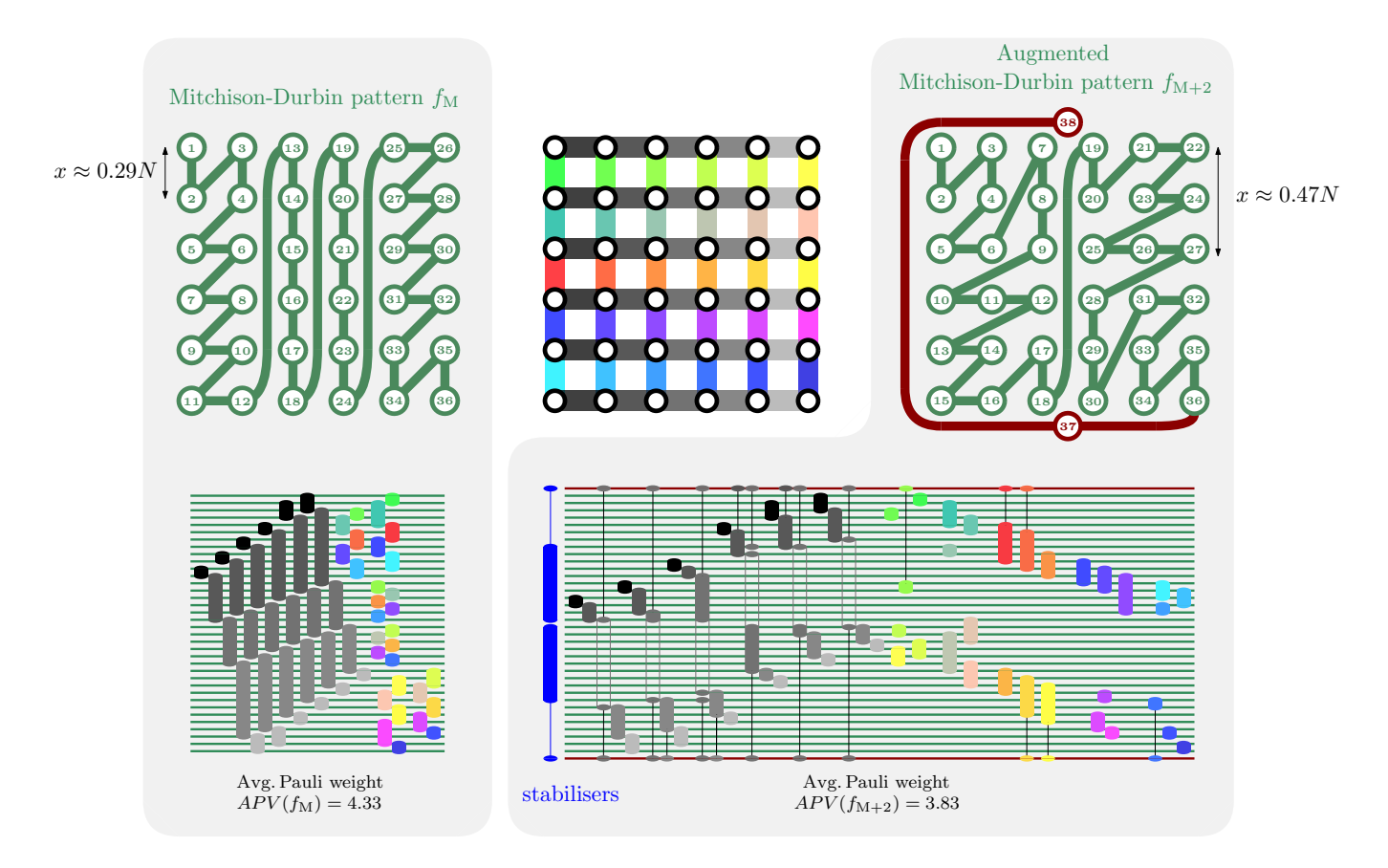


Figure 27: Comparison between the average Pauli weights of Jordan-Wigner mappings generated by the Mitchison-Durbin pattern $f_{\rm M}$ (left) and our auxiliary qubit pattern $f_{\rm M+2}$ (right). The bottom right image shows the reduction of the Pauli weight of long terms after multiplication by stabilisers. Terms that partially overlap the stabilisers must also be adjusted.

This analysis does not include the cost of initialising the stabiliser state $|\widetilde{\psi}\rangle_{\rm dat,aux}$ via the unitary operation V. It is possible to implement V using fewer gates than the circuit in Figure 25 at the cost of more ancilla qubits [37]. However, even adding the cost of the circuit in Figure 25, which is $4(xN-x^2+(x-1))+2$ CNOTs, to Equation 99 has negligible effects on the calculations in this section. The value $x\approx 0.47N$ in Equation 102, and limits in Equations 104 and 103, still hold.

Figure 26 shows the average Pauli weights of all the enumeration schemes for the $N \times N$ fermionic lattice discussed in this paper. It includes ' f_{M+1} ', our name for the auxiliary qubit mapping that arises if we use only one p-string in our protocol (and hence only one stabiliser, which would replace the factor of 2 in Equation 99 with a 1). This still outperforms the Mitchison-Durbin pattern.

Figure 27 concludes by demonstrating the advantage of our auxiliary qubit mapping on the 6×6 lattice. Substituting N=6, x=3 into Equation 100 yields a qubit Hamiltonian \widetilde{H} with a total Pauli weight of 230. The average Pauli weight is then $\frac{230}{60}=3.83$, which is an 11.5% improvement on the Mitchison-Durbin pattern's ancilla-free optimal average Pauli weight of 4.33 (total Pauli weight 260), and a 14.9% improvement on the S-and Z-patterns' average of 4.5 (total 270).

V. DISCUSSION

We have provided novel ways of improving on fermionqubit mappings by optimising the fermion enumeration schemes; Theorem 1 yields the optimal result for average Pauli weight in the case of fermionic lattices. We have also demonstrated an approach to hybridising our fermion enumeration scheme strategy with a constant number of ancilla qubits to further increase the locality of lattice Hamiltonians.

These techniques are remarkably general and reduce the length of all quantum circuits employing Jordan-Wigner type mappings. In Section VA, we situate our results within the existing literature. In Section VB, we show how our approach is compatible with other stateof-the-art approaches fermion-qubit mappings, many of which assume some underlying qubit architecture.

A. Fermion enumeration schemes in the context of quantum simulation

This section illustrates the context within which our result provides immediate practical value: the reduction of gate count in quantum algorithms for solving generic

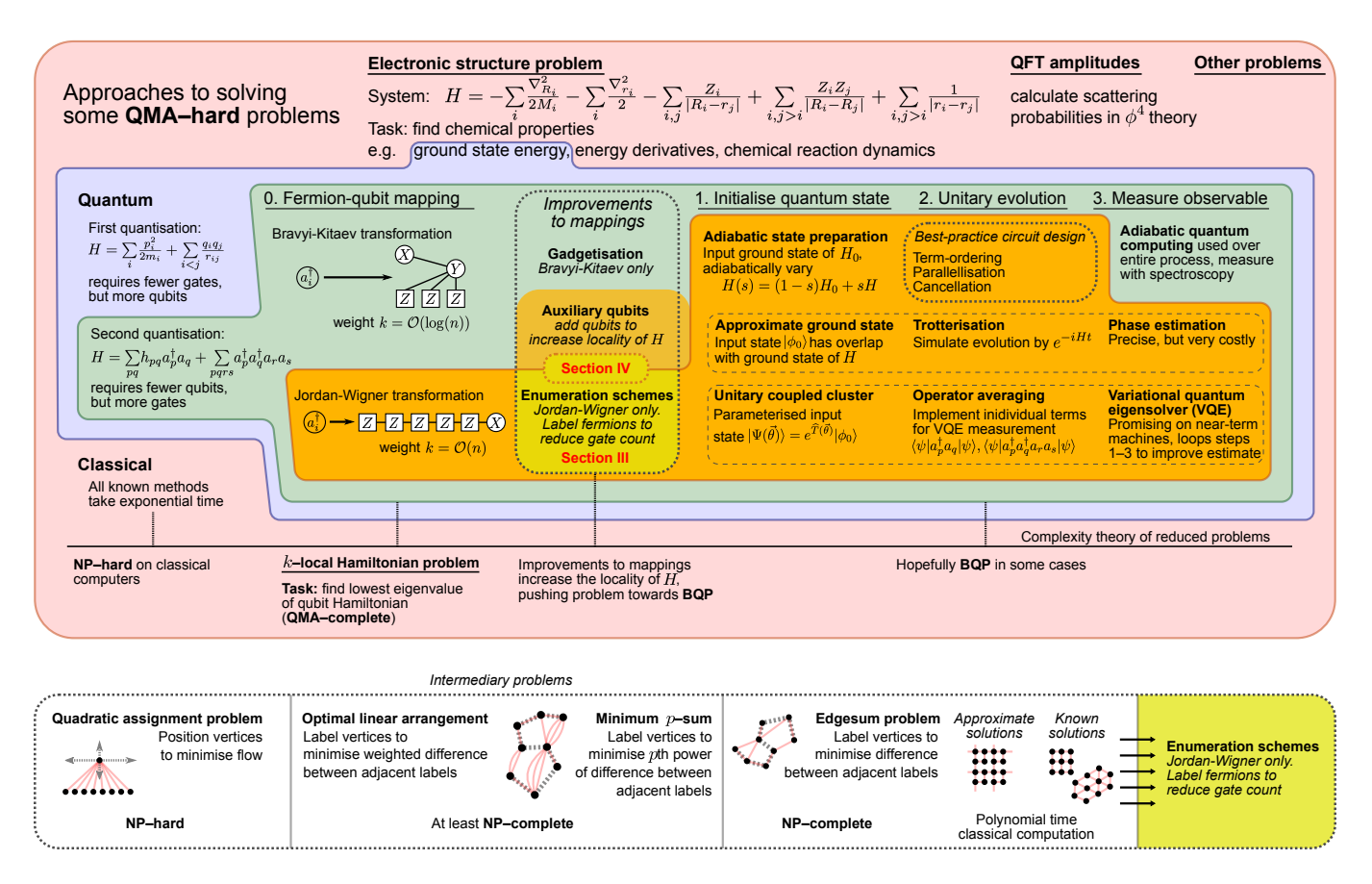


Figure 28: **Top:** (read columns left-to-right) broad overview of quantum algorithms for calculating fermionic properties, and where fermion enumeration and the contributions of Sections III and IV fit into such algorithms. **Bottom:** complexity-theoretic heirarchy of problems generalising the edgesum problem.

instances of quantum chemistry problems and beyond. Figure 28 offers a top-down summary of the state of the field and the precise place our techniques occupy in the context of simulating physical systems. We propose this diagram as a schematic of the suite of options available to a quantum computing engineer in the near-future, listing technologies (quantum or classical), methods (first- or second-quantisation), and algorithms (adiabatic, phase estimation, hybrid quantum-classical, among others), in order to solve an underlying problem (in this case, finding the ground state energy of a molecular Hamiltonian).

Brief note on Bravyi-Kitaev and other mappings. The search for more efficient mappings beyond the Jordan-Wigner transformation resulted in Bravyi-Kitaev type transformations [26], which yield to exponentially shorter Pauli strings in the asymptotic limit. The Bravyi-Kitaev transformation does not outperform Jordan-Wigner on modest fermionic systems, however, and has a similar T-gate count [38]. The Jordan-Wigner mapping has also gained a widespread use because it demands far fewer degrees of connectivity in the qubit architecture [16]. Authors have embedded the k-local Hamiltonian problems in higher-dimensional Hilbert spaces; through a process called gadgetisation in some Bravyi-Kitaev-based adiabatic quantum computing protocols [6], or through the

introduction of auxiliary qubits for both Bravyi-Kitaev [15, 18, 19] and Jordan-Wigner-type [12, 16, 36] mappings.

B. Compatibility with existing tools

Most of the results that have made use of the Jordan-Wigner and Bravyi-Kitaev transformations rely on qubits with a higher connectivity than the 1D array. In particular, Verstraete and Cirac [12] pursue a Jordan-Wigner type auxiliary qubit mapping to transform a local Hamiltonian on a fermionic lattice to a local Hamiltonian on a qubit lattice. Subsequent works have followed suit, usually working towards preserving geometric locality between the fermions and qubits, where the assumption is that the qubit architecture is the same as the fermionic graph [15, 16, 19, 36].

Our results are compatible with all existing qubit architectures. To see this, consider decomposing a fermion-qubit mapping from a fermionic graph $G_{\rm F}$ to a qubit graph $G_{\rm Q}$ into two components: 1) the enumeration of the fermions, which projects the fermionic connectivity graph $G_{\rm F}$ onto a 1D array of qubits, and then 2) the embedding of the 1D array of qubits into the qubit archi-

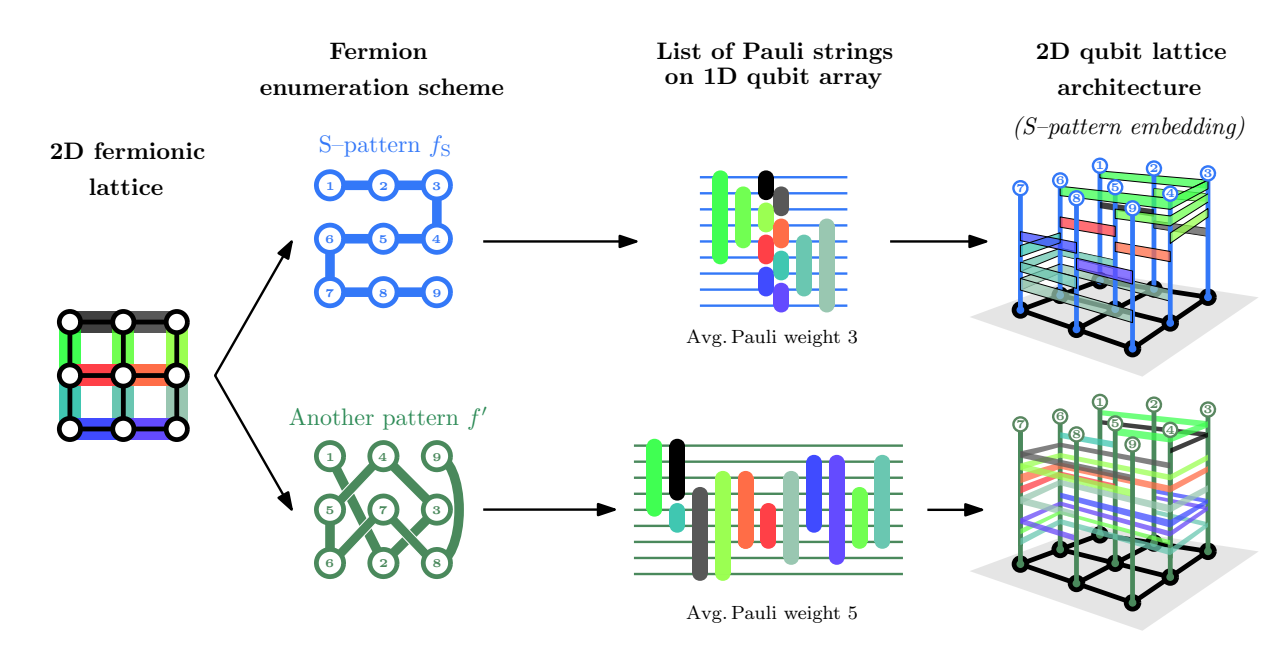


Figure 29: When working with elaborate qubit architectures such as the 2D lattice, the fermion enumeration scheme need not follow the underlying qubit connectivity. This figure highlights the freedom to choose any scheme to enumerate fermions, yielding averages for the Pauli weights independent of the actual qubit connectivity.

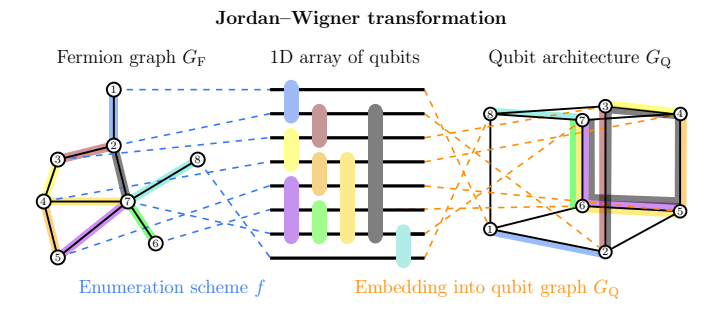


Figure 30: It is important to distinguish the choice of fermion enumeration scheme from the choice of Pauli string embedding. Only the latter is dependent on the qubit architecture.

tecture $G_{\mathbf{Q}}$. Figure 30 visualises the distinction between the two processes.

Verstraete and Cirac's approach is to introduce the S-pattern to enumerate the fermions, and to use an S-pattern embedding to weave Pauli strings into the qubit lattice, as in the top row of Figure 29. In this work we emphasise that these are two entirely separate processes, and the choice of fermion enumeration scheme can be done in an entirely separate way to the method of the embedding process. Indeed, as the second row of Figure 29 shows, the path of the fermion enumeration scheme need not follow the connectivity of the qubit architecture at all to provide a valid mapping.

In conclusion, to minimise the average Pauli weight of a Jordan-Wigner type mapping, the enumeration scheme that solves $G_{\rm F}$'s edgesum problem provides the optimal result, no matter the structure of the qubit architecture which will eventually implement the Pauli strings. Crucially, the improvement to a Jordan-Wigner transformation through the choice of an optimal fermion enumeration scheme comes at the cost of no extra resources. This distinguishes the result from other methods of improving fermion-qubit mappings such as the introduction of auxiliary qubits [12, 15, 16, 36].

It is possible to conceive of metrics for fermion enumeration scheme that do depend on qubit architectures. As mentioned in Section III A, one could penalise strings of Pauli gates that spread through the graph $G_{\rm Q}$ sparsely, and reward clustered Pauli strings. This poses a different problem and the 'optimal' enumeration scheme will need to take into account the qubit architecture as well. We expect that this is a much more difficult problem to solve than minimising average Pauli weight through solutions to the edgesum problem.

Acknowledgements MC is funded by Cambridge Australia Allen and DAMTP Scholarship and the Royal Society PhD studentship. SS acknowledges support from the Royal Society University Research Fellowship scheme.

VI. APPENDIX

A. Edgesum of the S-pattern

Lemma 6. On an $N \times N$ lattice, the S-pattern f_S has edgesum $C^1(f_S) = N^3 - N$.

Proof. Figure 31 displays the S–pattern enumeration procedure for an $N \times N$ grid, as well as the differences be-

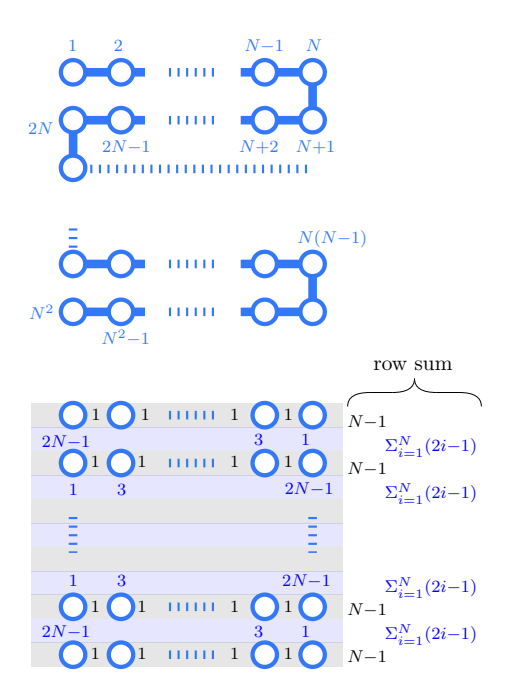


Figure 31: **Top:** S-pattern enumeration on the $N \times N$ square lattice. **Bottom:** Differences between vertex labels using the S-pattern enumeration, with row totals on the far right.

tween adjacent vertices' indices.

Regardless of whether N is odd or even, the cost is thus

$$C^{1}(f_{S}) = (N-1) \times \text{no. of rows}$$

$$+ \sum_{i=1}^{N} (2i-1) \times (\text{no. of rows} - 1)$$

$$= N^{2} - N + (N-1)(N(N+1) - N)$$

$$= N^{2} - N - N^{2} + N + N(N^{2} - 1)$$

$$= N^{3} - N.$$

$$(105)$$

The average Pauli weight for the S–pattern on a square lattice is then

$$APV(f_{S}) = \frac{C^{1}(f_{S})}{|E|} + 1 = \frac{N^{3} - N}{2N(N - 1)} + 1 \qquad (108)$$
$$= \frac{1}{2}N + \frac{3}{2}. \qquad (109)$$

- Alán Aspuru-Guzik, Anthony D Dutoi, Peter J Love, and Martin Head-Gordon. Simulated quantum computation of molecular energies. *Science*, 309(5741):1704–1707, 2005
- [2] Jarrod R McClean, Ryan Babbush, Peter J Love, and Alán Aspuru-Guzik. Exploiting locality in quantum computation for quantum chemistry. *The journal of physical* chemistry letters, 5(24):4368–4380, 2014.
- [3] Ivan Kassal, Stephen P Jordan, Peter J Love, Masoud Mohseni, and Alán Aspuru-Guzik. Polynomial-time quantum algorithm for the simulation of chemical dynamics. *Proceedings of the National Academy of Sciences*, 105(48):18681–18686, 2008.
- [4] Ivan Kassal and Alán Aspuru-Guzik. Quantum algorithm for molecular properties and geometry optimization. The Journal of chemical physics, 131(22):224102, 2009.
- [5] Gerardo Ortiz, James E Gubernatis, Emanuel Knill, and Raymond Laflamme. Quantum algorithms for fermionic simulations. *Physical Review A*, 64(2):022319, 2001.
- [6] Ryan Babbush, Peter J Love, and Alán Aspuru-Guzik. Adiabatic quantum simulation of quantum chemistry. Scientific reports, 4(1):1–11, 2014.
- [7] Hefeng Wang, Sabre Kais, Alán Aspuru-Guzik, and Mark R Hoffmann. Quantum algorithm for obtaining the energy spectrum of molecular systems. *Physical Chemistry Chemical Physics*, 10(35):5388–5393, 2008.
- [8] A Yu Kitaev. Quantum measurements and the abelian stabilizer problem. arXiv preprint quant-ph/9511026, 1995.
- [9] Daniel S Abrams and Seth Lloyd. Quantum algorithm providing exponential speed increase for finding eigenvalues and eigenvectors. *Physical Review Letters*,

83(24):5162, 1999.

- [10] Alberto Peruzzo, Jarrod McClean, Peter Shadbolt, Man-Hong Yung, Xiao-Qi Zhou, Peter J Love, Alán Aspuru-Guzik, and Jeremy L O'brien. A variational eigenvalue solver on a photonic quantum processor. *Nature commu*nications, 5(1):1–7, 2014.
- [11] Jarrod R McClean, Jonathan Romero, Ryan Babbush, and Alán Aspuru-Guzik. The theory of variational hybrid quantum-classical algorithms. New Journal of Physics, 18(2):023023, 2016.
- [12] Frank Verstraete and J Ignacio Cirac. Mapping local hamiltonians of fermions to local Hamiltonians of spins. Journal of Statistical Mechanics: Theory and Experiment, 2005(09):P09012, 2005.
- [13] Ivan Kassal, James D Whitfield, Alejandro Perdomo-Ortiz, Man-Hong Yung, and Alán Aspuru-Guzik. Simulating chemistry using quantum computers. Annual review of physical chemistry, 62:185–207, 2011.
- [14] Julia Kempe, Alexei Kitaev, and Oded Regev. The complexity of the local Hamiltonian problem. Siam journal on computing, 35(5):1070–1097, 2006.
- [15] Charles Derby and Joel Klassen. Low weight fermionic encodings for lattice models. arXiv preprint arXiv:2003.06939, 2020.
- [16] Mark Steudtner and Stephanie Wehner. Quantum codes for quantum simulation of fermions on a square lattice of qubits. *Physical Review A*, 99(2):022308, 2019.
- [17] Pascual Jordan and Eugene Wigner. Über das Paulische Äquivalenzverbot. Zeitschrift fur Physik, 47(9-10):631–651, September 1928.
- [18] Kanav Setia, Sergey Bravyi, Antonio Mezzacapo, and James D Whitfield. Superfast encodings for

- fermionic quantum simulation. Physical Review Research, 1(3):033033, 2019.
- [19] Zhang Jiang, Jarrod McClean, Ryan Babbush, and Hart-mut Neven. Majorana loop stabilizer codes for error mitigation in fermionic quantum simulations. *Physical Review Applied*, 12(6):064041, 2019.
- [20] Zhang Jiang, Amir Kalev, Wojciech Mruczkiewicz, and Hartmut Neven. Optimal fermion-to-qubit mapping via ternary trees with applications to reduced quantum states learning. *Quantum*, 4:276, June 2020.
- [21] Graeme Mitchison and Richard Durbin. Optimal numberings of an N×N array. SIAM Journal on Algebraic Discrete Methods, 7(4):571–582, 1986.
- [22] Michael R Garey, David S Johnson, and Larry Stockmeyer. Some simplified NP-complete problems. In Proceedings of the sixth annual ACM symposium on Theory of computing, pages 47–63, 1974.
- [23] Michael R Garey, Ronald L Graham, David S Johnson, and Donald Ervin Knuth. Complexity results for bandwidth minimization. SIAM Journal on Applied Mathematics, 34(3):477–495, 1978.
- [24] Michael R Garey and David S Johnson. Computers and Intractability; A Guide to the Theory of NP-Completeness. W. H. Freeman & Co., USA, 1990.
- [25] Michael A Nielsen et al. The fermionic canonical commutation relations and the Jordan-Wigner transform. School of Physical Sciences The University of Queensland, 59, 2005.
- [26] Sergey B Bravyi and Alexei Yu Kitaev. Fermionic quantum computation. Annals of Physics, 298(1):210–226, 2002.
- [27] Tjalling C Koopmans and Martin Beckmann. Assignment problems and the location of economic activities. Econometrica: journal of the Econometric Society, pages 53–76, 1957.
- [28] Steven Bradish Horton. The optimal linear arrangement problem: algorithms and approximation. PhD thesis, School of Industrial and Systems Engineering, Georgia Institute of Technology, 1997.
- [29] Martin Juvan and Bojan Mohar. Optimal linear labelings and eigenvalues of graphs. Discrete Applied Mathematics, 36(2):153–168, 1992.
- [30] Alan George and Alex Pothen. An analysis of spectral envelope reduction via quadratic assignment problems. SIAM Journal on Matrix Analysis and Applications, 18(3):706-732, 1997.
- [31] Yung-Ling Lai and Kenneth Williams. A survey of solved problems and applications on bandwidth, edgesum, and profile of graphs. *Journal of graph theory*, 31(2):75–94, 1999.
- [32] Greg N Frederickson and Susanne E Hambrusch. Planar linear arrangements of outerplanar graphs. *IEEE transactions on Circuits and Systems*, 35(3):323–333, 1988.
- [33] Fan-Rong King Chung. On optimal linear arrangements of trees. Computers & mathematics with applications, 10(1):43-60, 1984.
- [34] James B Saxe. Dynamic-programming algorithms for recognizing small-bandwidth graphs in polynomial time. SIAM Journal on Algebraic Discrete Methods, 1(4):363–369, 1980.
- [35] Nikolaj Moll, Andreas Fuhrer, Peter Staar, and Ivano Tavernelli. Optimizing qubit resources for quantum chemistry simulations in second quantization on a quantum computer. Journal of Physics A: Mathematical and

- Theoretical, 49(29):295301, 2016.
- [36] James D Whitfield, Vojt ĕch Havlíček, and Matthias Troyer. Local spin operators for fermion simulations. Phys. Rev. A, 94:030301, Sep 2016.
- [37] Jiaqing Jiang, Xiaoming Sun, Shang-Hua Teng, Bujiao Wu, Kewen Wu, and Jialin Zhang. Optimal space-depth trade-off of CNOT circuits in quantum logic synthesis. In Proceedings of the Fourteenth Annual ACM-SIAM Symposium on Discrete Algorithms, pages 213–229. SIAM, 2020.
- [38] Andrew Tranter, Peter J Love, Florian Mintert, and Peter V Coveney. A comparison of the bravyi–kitaev and jordan–wigner transformations for the quantum simulation of quantum chemistry. *Journal of chemical theory and computation*, 14(11):5617–5630, 2018.